DEUTSCHES ELEKTRONEN-SYNCHROTRON DESY

DESY 72/61
October 1972

Recent Developments in Electro- and Photoproduction

by

Günter Wolf

2 HAMBURG 52 · NOTKESTIEG 1

Recent Developments in Electro- and Photoproduction

GÜNTER WOLF

Deutsches Elektronen-Synchrotron, DESY, Hamburg

Lecture notes for the International School of Elementary Particle Physics, Basko Polje - Makarska (Yugoslavia).

This lecture will cover three areas of photo- and electroproduction, for which new results have been obtained since the 1971 Cornell conference[1]. These are the ρ', rho electroproduction and the Q^2 dependence of the multiplicities and inclusive particle spectra.

1. A new vectorstate, the ρ'

In the framework of the vector dominance model (VDM) the photon, or equivalently the electromagnetic current, $j_\mu(x)$, when interacting with hadrons can be described by the fields of ρ, ω and ϕ [2]:

$$j_\mu(x) = -e\left\{\frac{M_\rho^2}{2\gamma_\rho}\rho_\mu(x) + \frac{M_\omega^2}{2\gamma_\omega}\omega_\mu(x) + \frac{M_\phi^2}{2\gamma_\phi}\phi_\mu(x)\right\}$$

where M_V ($V = \rho, \omega, \phi$) is the vector meson mass and γ_V measures the γ-V coupling strength:

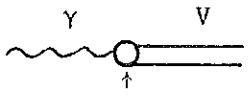

$$\frac{eM_V^2}{2\gamma_V} \equiv \sqrt{\alpha\pi}\,\frac{M_V^2}{\gamma_V}$$

This conjecture has greatly stimulated the study of photon hadron interactions and has proven to be a useful guide for understanding many of the phenomena observed. One of the possible applications of Eq(1) is to relate the Compton amplitude to transverse vector meson photoproduction:

$$T_{\gamma p \to \gamma p} = \sum_{V=\rho,\omega,\phi} \frac{\sqrt{\alpha\pi}}{\gamma_V} T^{\text{trans}}_{\gamma p \to Vp} \qquad (2)$$

or diagrammatically

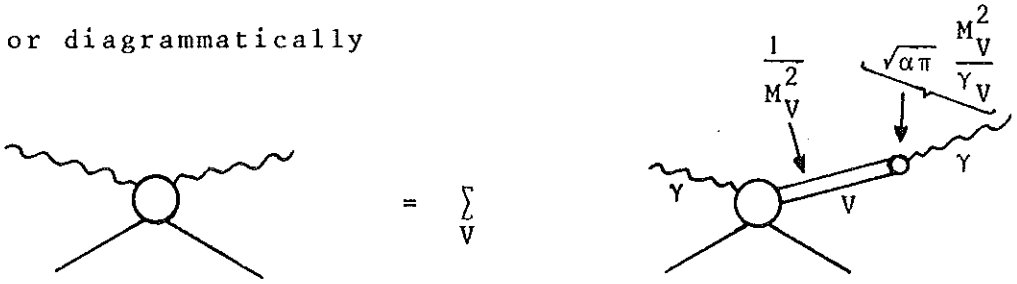

Using the γ_V values determined at Orsay[3] and Novosibirsk[4] from e^+e^- annihilation, $e^+e^- \to V$, and the measured cross sections for $\gamma p \to Vp$ it turned out, that ρ,ω and ϕ in Eq(2) contributed only ~70 % of the Compton amplitude[5,6]. Difficulties with VDM were also encountered in other areas such as the nulceon electromagnetic formfactor. One of the remedies proposed was the addition of further vector mesons which yet had to be discovered. Extensive searches for such mesons were unsuccessful until this year when at Frascati[7] in a study of e^+e^- annihilation and by a Berkeley-SLAC Collaboration[8] analyzing the reaction

$$\gamma p \to p 2\pi^+ 2\pi^- \qquad (3)$$

a 4π vector state of mass ~1.5 GeV was discovered. Actually the first ones to observe a 4π enhancement in reaction (3) in this mass region were Davier et al. in a streamer chamber experiment at SLAC[9].

Fig. 1 shows the evidence from Frascati[10] for the so called ρ' in the $2\pi^+2\pi^-$ system.
The data from the Berkeley-SLAC collaboration resulted from a 250 events/μb bubble chamber exposure. The photon beam was linearly polarized and had an energy of 9.3 GeV. Fig. 2 shows some of the mass distributions observed for reaction (3).
A distinct enhancement in the 4π mass distribution near ~1.5 GeV is seen after the Δ^{++} events (see Fig.2b) have been removed (shaded histogram in Fig.2a). The experiment established that the charged four-pion final state is reached via decay into $\rho^o + \sigma$, where σ denotes a isospin zero s-wave $\pi^+\pi^-$ system.

In the e^+e^- annihilation experiment spin and parity follow directly from the assumption of one-photon exchange, i.e. $J^P_{\rho'} = 1^-$. In the γp experiment the J^P assignment was obtained from a study of the decay angular distribution of the ρ' with respect to the photon polarization vector ε. In searching for an alignment of the ρ' with respect to ε the trick was to group the four pions into $(\pi^+\pi^+)$ and $(\pi^-\pi^-)$. The handwaving argument for such a grouping goes as follows. Because of Bose-statistics the possible states for these subsystems are $J^P = 0^+, 2^+, 4^+ \ldots$. Suppose that $J^P_{\rho'} = 1^-$ and both subsystems are in a 0^+ state. Then $(\pi^+\pi^+)$ and $(\pi^-\pi^-)$ will be in relative p-wave state:

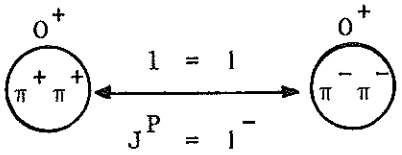

The situation is now similar to ρ^o photoproduction with the π^+ (from $\rho^o \to \pi^+\pi^-$) being replaced by the vector $\vec{Q} = \vec{\pi}^+ + \vec{\pi}^+$. From the results on ρ^o photoproduction[11] we expect the ρ' spin to be aligned along its direction of flight in the total cms, therefore,

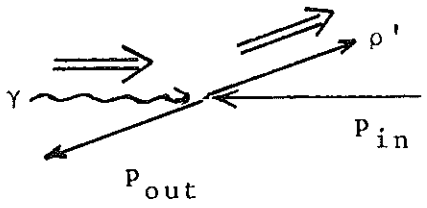

with the definition of angles given below (for <u>forward</u> produced ρ') the vector $\vec{Q}$ will lie preferentially <u>in</u> the plane of photon polarization (i.e. $\psi = 0^o, 180^o$) and will show a $\sin^2\Theta$ distribution for the polar angle Θ in the ρ' rest system.

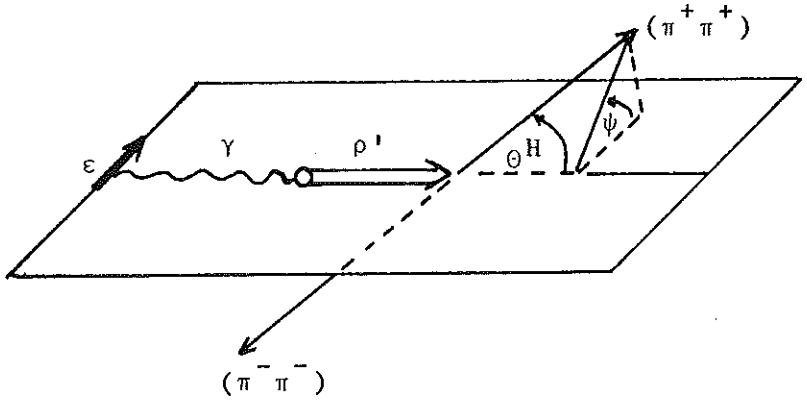

Figs. 3a,b show that such a behaviour – at least qualitatively – is indeed observed. In reality the angular momentum states of the $(\pi^+\pi^+)$ and $(\pi^-\pi^-)$ are more complicated (e.g. to form a ρ^o_σ state) than assumed above. A detailed analysis done by the authors of Ref. 8 showed that the $J^P = 1^-$ assignment was strongly favored by the data.

It should be noted that neither the annihilation nor the photoproduction experiment can decide on whether the ρ' is a resonance or a continuum. A possible way of distinction is to measure $\gamma p \to p\rho' \hookrightarrow e^+e^-$ and to look for an interference with Bethe-Heitler e^+e^- pair production.

In Table I the observed properties of the ρ' are collected. Assuming that the ρ'-nucleon and ρ nucleon elastic cross sections are equal and that $\sigma(\rho' N \to \rho N) << \sigma(\rho' N \to \rho' N)$, one can deduce the $\gamma_{\rho'}$ coupling strength via VDM:

$$(\gamma_{\rho'}/\gamma_\rho)^2 = \sigma(\gamma p \to \rho p)/\sigma(\gamma p \to \rho' p)$$

$$= 6 \pm 2 \text{ at } 9.3 \text{ GeV}$$

or $$\gamma_{\rho'}{}^2/4\pi = 3.9 \pm 1.3$$

Here we have assumed that the ρ' decays only into $\rho^o\sigma$. The value for $(\gamma_{\rho'}/\gamma_\rho)^2$ is in fair agreement with the annihilation result of ≈ 4.

Finally, let us see to what extent the ρ' contribution improves the Compton sum rule. An evaluation of Eq(2) at $E_\gamma = 9.3$ GeV using the input values listed in Table 2 and neglecting possible real parts leads to (in $(\mu b/GeV^2)^{1/2}$):

$$0.87 \pm 0.02 = (0.52 \pm 0.04) + (0.066 \pm 0.014) + (0.043 \pm 0.004) + (0.084 \pm 0.03) = 0.71 \pm 0.05$$

$\gamma p \to \gamma p$ $\quad$ $\gamma p \to \rho^o p$ $\quad$ $\gamma p \to \omega p$ $\quad$ $\gamma p \to \phi p$ $\quad$ $\gamma p \to \rho' p$

Still further vector mesons are needed to satisfy Eq(2).[7]

II. Electroproduction

The electroproduction data will be discussed in terms of the standard variables:

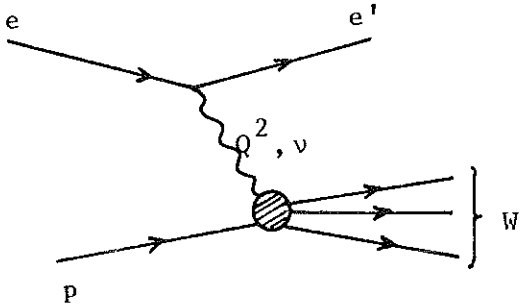

$e = (\vec{e}, E)$, $e' = (\vec{e}', E')$	four momenta of the incoming and scattered electrons
$\Theta =$	e' scattering angle in the Lab.system
$p = (0, m_p)$	target proton
$-Q^2 = (e-e')^2 = -4EE' \sin^2\frac{\Theta}{2}$	mass squared of virtual photon
$\nu = E - E'$	Lab. energy of virtual photon
$W^2 = (e-e'+p)^2$ $= 2m_p\nu + m_p^2 - Q^2$	mass squared of outgoing hadron system

For virtual photons ($-Q^2 < 0$) the photon polarization vector has a transverse as well as a longitudinal component. In the notation of Hand[14] the differential cross section for electroproduction, $d^2\sigma/dQ^2dW$, is expressed in terms of the cross sections σ_T and σ_L, for scattering of transverse and longitudinal photons:

$$\frac{d^2\sigma}{dQ^2dW} = \frac{\pi}{EE'}\frac{W}{m_p}\Gamma_T\{\sigma_T(Q^2,W) + \varepsilon\,\sigma_L(Q^2,W)\} \qquad (4)$$

with the transverse flux, Γ_T, being defined as

$$\Gamma_T = \frac{\alpha}{4\pi^2}\frac{E'}{E}\frac{W^2 - m_p^2}{m_p\,Q^2}\frac{1}{1-\varepsilon}$$

and $\varepsilon = [1 + 2(Q^2 + \nu^2)\, Q^{-2}\, tg^2 \frac{\Theta}{2}]^{-1}$

Much of the experimental work at electron accelerators is now concentrated on the study of inelastic electron and muon scattering in an effort to understand the cross section observed in the deep inelastic region[15,16]. While the nucleon electromagnetic formfactors fall rapidly with Q^2 ($-Q^2$ = mass squared of the virtual photon) the total inelastic ep scattering cross section decreases only slowly with Q^2 (see Fig.4) and appears to have a pointlike behaviour. This observation spurred experimenters to measure individual inelastic channels in order to see whether the observed Q^2 behaviour is caused by specific final states. A number of measurements have been carried out at Cornell, DESY and NINA on pseudoscalar meson production, e.g. $ep \to e\pi N$, $e\pi\Delta$, $eK\Lambda$ etc.[19], most of which have been reviewed by Berkelman and by Toner[20]. I shall discuss new data on inclusive spectra and preliminary results from two experiments, one at DESY, one at SLAC, where <u>all</u> charged particles in the final state are observed. Since the latter two experiments use new types of techniques a short description of the experimental setup is given.

Fig. 5 shows the layout of the DESY streamer chamber experiment.[18] A 7.2 GeV electron beam strikes a liquid hydrogen target inside a streamer chamber. The chamber is placed in a magnet. A hodoscope of scintillation and shower counters taggs the scattered electron. If a scattered electron has been detected a photograph of the chamber is taken. Fig. 6 shows a picture. The kinematically accepted region is $0.3 < Q^2 < 2$ GeV^2, $W < 2.7$ GeV. It takes approximately $5 \cdot 10^7$ incident electrons for one event and the data rate is 50-100 events/hour. Sofar results from 5100 events have been reported of which 2300 have 3 or more charged outgoing hadrons.

The SLAC μp bubble chamber experiment is shown in Fig. 7. A 16 GeV μ^- beam (~100 μ's per pulse) passes through the SLAC 40-inch hydrogen bubble chamber which is operated in a rapid cycling mode (10pps). The muon detector consists of an iron-scintillator sandwich plus spark chambers. One inelastic μ event requires roughly $6 \cdot 10^3$ expansions corresponding to ~6 events/hour. Data are available from 2300 inelastic events in the region $0.15 < Q^2 < 3\ \mathrm{GeV}^2$, $1.4 \leq W \leq 3.8$ GeV.

1. Electroproduction of ρ^o mesons, $ep \to ep\rho^o$

There are many interesting aspects about ρ^o electroproduction: a) VDM links this process to virtual Compton scattering, $\gamma_V p \to \gamma_V p$ (see Eq(2)), and, through the optical theorem, to the total inelastic cross section; b) the ρ^o decay distribution gives us insight in the spin dependence of the production process and we can check whether ρ^o production with virtual photons conserves the s-channel cms helicity (SCHC) as well as in photoproduction; c) The ratio of the production cross sections σ_L, σ_T by longitudinal and transverse photons has been predicted to increase rapidly with Q^2: [22]

$$\sigma_L(ep \to ep\rho^o) \simeq \frac{Q^2}{m_\rho^2}\ \sigma_T(ep \to ep\rho^o)$$

This has to be contrasted with the empirical fact $\sigma_L/\sigma_T \lesssim 0.2$ for the total inelastic scattering[15,17,23]. d) It has been suggested that the hadronic interaction radius of the photon shrinks[24] as Q^2 increases. As a consequence the momentum transfer distribution of electroproduced ρ^o mesons should become wider for larger Q^2.

Rho production leads to the final state $ep\pi^+\pi^-$. Fig. 8 shows the cross section for this reaction as a function of W in different Q^2 intervals.[18] Qualitatively the same W dependence is observed as in photoproduction.[25] The Q^2 dependence of the cross section for $ep\pi^+\pi^-$ is approximately the same as that of

the total inelastic cross section (Fig. 9). Figs. 10-14 show the $\pi^+ p$ and $\pi^+\pi^-$ mass distributions for different W intervals as measured in the DESY streamer chamber experiment[18] (Fig. 10-12), in the SLAC μp HBC experiment[21] (Fig. 13) and in an ep spark chamber experiment at SLAC[26] (Fig. 14). The low W region ($W < 1.7$ GeV) is dominated by Δ^{++} production, the region $W > 2$ GeV by ρ^o production. Fig. 15 shows the $(\rho + \omega)$ signal obtained in a missing mass experiment, $ep \to ep + MM$[27]. The Q^2 dependence of the ρ^o cross section is shown in Fig. 16. For $W > 2$ GeV the ρ^o cross section drops much faster with Q^2 than does the total inelastic cross section (dashed-dotted curve). The ratio σ_ρ/σ_{tot} drops from 16 ± 0.5 % at $Q^2 = 0$ [11] to 4 ± 2 % at $Q^2 = 1.1$ GeV^2 (Ref. 18), see Table 3.

Approximately 30 % of this decrease is due to the t_{min} cutoff, where t is the four momentum transfer between incoming and outgoing proton

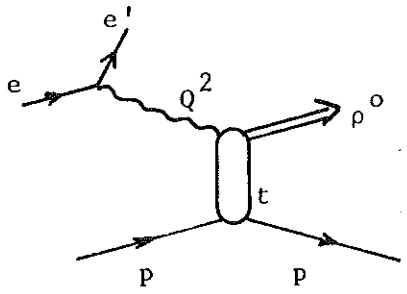

and very crudely $|t|_{min} \simeq \left(\frac{Q^2 + m_\rho^2}{2\nu}\right)^2$. The effect of the t_{min} cutoff is indicated by the open circles which show σ_ρ multiplied by $e^{A|t|_{min}}$ ($A = 6$ GeV^{-2} for $Q^2 = 0$, $A = 4$ GeV^{-2} for $Q^2 > 0$).

t-dependence.

Sofar no experiment has determined the t dependence of the ρ cross section the way it should be done, namely by fitting the amount of ρ production in each t bin separately (mainly because of limited statistics). Instead, the t behaviour was obtained by taking all events in the ρ region.

Fig. 17 shows $d\sigma/dt$ versus t for different Q^2 intervals together with photoproduction data which were obtained in the same way. The t distributions flatten as Q^2 increases. A similar trend is observed in the other experiments (see Fig.18). In Table 4 the results from exponential fits to the t distributions have been collected. Possible reasons for the decreasing slope of the t distribution with larger Q^2 are

- more background under the ρ at higher t and Q^2;
- large longitudinal ρ cross section with different t behaviour;
- large real part at large t and Q^2;
- the photon shrinks.

We ignore for a moment the first three points and try to see whether the observed slope values would fit into the picture of a shrinking photon. A suitable variable for studying the slope $A_{\rho p}$ is the time $\Delta\tau$ which the photon may spend as a rho meson. From the uncertainty principle we get $\Delta\tau = (E_\rho - \nu)^{-1} \simeq 2\nu/(Q^2 + m_\rho^2)$. In Fig.19 the slope values have been plotted versus $\Delta\tau$. We expect for $\Delta\tau = 0$: $A_{\rho p} \simeq \frac{1}{4}A_{pp}$ where A_{pp} is the slope for elastic pp scattering, and for large $\Delta\tau$: $A_{\rho p} \simeq A_{\pi p}$. The data do not contradict this conjecture.

Decay distribution

The decay distribution for ρ events has been analyzed in the helicity system. The decay angles Θ_H (polar angle) and ψ_H (polarization angle) are defined in Fig. 20 (for forward produced ρ's). As a reminder Fig. 21 shows the distribution of $\cos\Theta_H$ and ψ for ρ^o mesons produced with linearly polarized photons[11]. An almost pure $\sin^2\Theta\cos^2\psi$ distribution due to s-channel helicity conservation (SCHC) is observed.

In electroproduction both transverse (γ_T) and longitudinal (γ_L) photons can contribute. The transverse photons are linearly polarized with the degree of polarization equal to ε. The polarization vector is in the electron scattering plane. If only γ_L contributes and SCHC holds then again a $\sin^2\Theta\cos^2\psi$ distribution will be observed. (ε is close to one in all of the experiments discussed here.) If the rhos are produced only by γ_L there will be no anisotropy around the ρ direction with respect to the electron scattering plane, i.e. $W(\psi_H) \sim$ const. If SCHC holds then $W(\cos\Theta) \sim \cos^2\Theta_H$.

γ_T + SCHC:

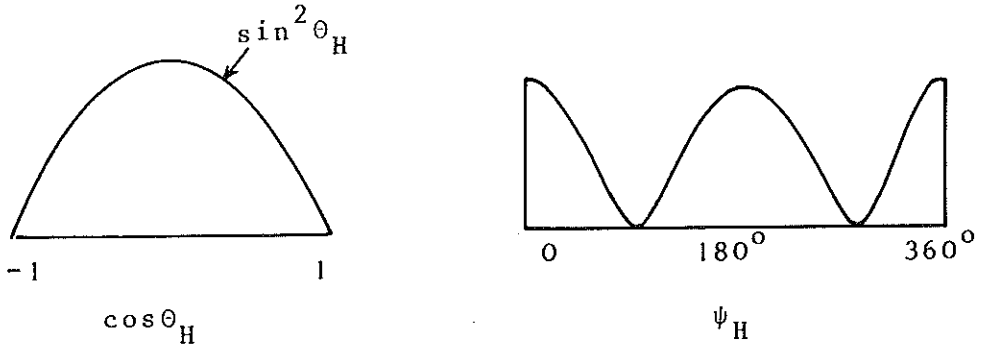

γ_L + SCHC:

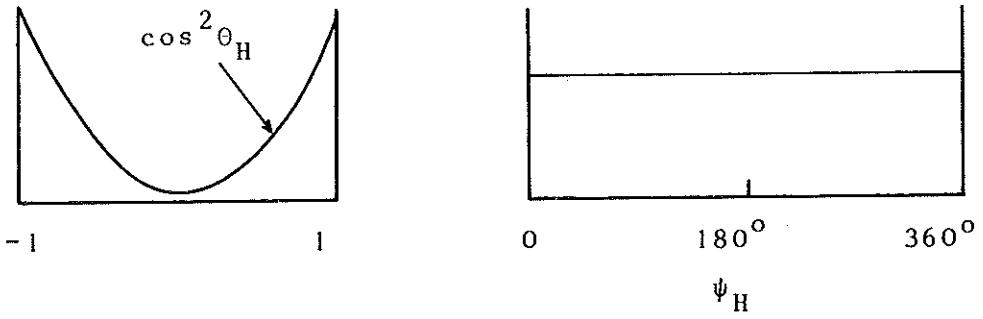

In general ρ production can have contributions from both, γ_T and γ_L and there may even be an interference between both.

Figs. 22 and 23 show the $\cos\Theta_H$ and ψ_H distributions for all events in the rho region. The $\cos\Theta_H$ distribution is flat indicating the production of both transverse and longitudinal ρ's; $W(\psi_H)$ has a strong $\cos^2\psi$ component which can only come from production by γ_T. The density matrix elements in the helicity frame as obtained by Ref. 18 are listed in Table 5. Also shown are the values expected for SCHC and $R_\rho = \sigma_L(\rho)/\sigma_T(\rho) = 0.6$. The data are consistent with SCHC. If one assumes SCHC from the $\cos\Theta_H$ distribution one can deduce the value of R_ρ. The result is $R_\rho = 0.6 \pm 0.2$. Background corrections due to Δ^{++} reflection may reduce the value of R_ρ somewhat.

2. ω-production

First results on muon produced ω mesons,

$$\mu p \rightarrow \mu p \omega \rightarrow \mu p \pi^+ \pi^- \pi^o$$

have been obtained in the SLAC experiment and are shown in Fig. 24. For small Q^2 a clear ω signal is seen.

3. Multiplicities for charged hadron production.

The track chamber experiments at DESY and SLAC have measured the average number $\langle n \rangle$ of charged hadrons produced as a function of Q^2 and W (Fig. 25). For $W \geq 2$ GeV a 10-20 % decrease of $\langle n \rangle$ is observed between $Q^2 = 0$ and ≈ 1 GeV^2.

4. Inclusive particle spectra

Several experiments have been focused on the Q^2 variation of inclusive π,k,p momentum and angular spectra. The results are usually presented in terms of the transverse momentum p_T and the Feynman variable $x = p^*_{\parallel}/p^*_{max}$ where $p^*_{\parallel}$ and p^*_{max} are the longitudinal and maximum possible momentum in the cms for the particle in question. All quantities refer to the process

$$\gamma_{Virtual} + p \rightarrow \text{hadrons}.$$

At <u>high</u> energies we expect to find three distinct x regions with qualitatively different behaviour:

- $x \approx -1$ particles from target fragmentation
- $x \approx +1$ particles from beam fragmentation
- $x \simeq 0$ central region with particles coming - in terms of the multiperipheral model - from the middle rungs.

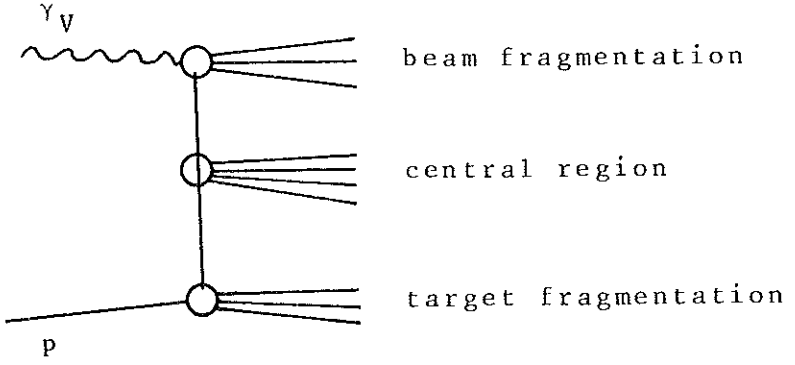

With this picture in mind we expect e.g. the pion distribution in the target region to be independent of the nature of the beam particle. Applied to electroproduction, at large energies the pion distribution for $x < 0$ should not depend on Q^2. Note, however, that the present experiments have been done at comparatively low energies, where the different regions overlap. For this reason the results may not be as clear cut.

a) $\pi^{\pm}$ spectra, general characteristics

In Fig. 26 the $\pi^{\pm}$ transverse momentum distributions in the photon fragmentation are shown for photo- and electroproduction as measured at DESY.[29,30] The quantity f shown is the invariant cross section,

$$f \equiv E \frac{d^3\sigma}{dp^3} .$$

We see that the average slope of the p_T^2 distributions decreases significantly with increasing Q^2.

No Q^2 dependence of the p_T distribution for $x \approx 0$ (i.e. central region) has been observed in a Cornell experiment[31] (see Fig.27).

In Fig. 28 the π^- distribution integrated over p_T is given for different Q^2 intervals[18] and compared with photoproduction[29]. While there is no change for $x < 0,2$ the π^- yield drops by a factor of 2-4 for large x. The dashed curves show the π^- yield for $Q^2 = 0$ after ρ^o events ($\gamma p \to \rho^o p$) have been removed. At $Q^2 = 0$ most of the π^- at large x are seen to come from ρ^o production. The dashed curves seem to follow closely the electroproduction points. Since, as we saw above, the fraction of ρ^o production drops rapidly with Q^2, the reduction in π^- yield can largely be understood in terms of the diminishing ρ^o cross section.

b) $\pi^{\pm}$ spectra at $p_T \approx 0$

The π^- and π^+ yields in the forward direction measured at DESY for photo-[32] and electroproduction ($Q^2 = 1.16$ GeV^2) [33] are compared in Figs. 29, 30.

A considerable drop in $\pi^{\pm}$ yield is observed for $x \gtrsim 0.2$. Furthermore, while the π^+ and π^- yields are roughly equal at $Q^2 = 0$ the π^+ are more abundant by a factor of ~2 for $x > 0.4$ and $Q^2 = 1.16$ GeV^2. The dashed curves in Figs. 29, 30 show the $\pi^{\pm}$ yields at $Q^2 = 0$ after removal of the ρ^o contribution[34]. Again, part of the observed Q^2 variation can be ascribed to the ρ^o. Another clue comes from the mass spectrum of the "missing" particle system opposite to $\pi^{\pm}$,

$$\gamma_V p \rightarrow \pi^{\pm} + MM$$

which is shown in Fig. 31 for $Q^2 = 1.16$ GeV^2 (Ref. 33). Low missing masses correspond to large values of x. The electroproduced π^+ at large x are seen to come mainly from two-body channels, such as

$$\gamma_V p \rightarrow \pi^+ n,\ \pi^+ \Delta^o,\ \pi^+ N^*(1520)$$

The only channel of this kind accessible to π^- production is $\gamma_V p \rightarrow \pi^- \Delta^{++}$. The main features of the Q^2 dependence observed for π^+ and π^- production can hence be understood as a consequence of the reduction in ρ^o production and of the increasing importance of the two-body reactions $\gamma_V p \rightarrow \pi^+$ Baryon.

The Q^2 dependence of the π^- and π^+ yield is shown in Fig. 32. The π^+/π^- ratio increases with Q^2. A similar increase of positive hadron yield over negative hadron yield has been observed in a SLAC experiment (Ref. 26).

c) K^+ spectra

A comparison of the K^+ yield in the forward direction at $Q^2 = 0$ (Ref. 32) and 1.16 GeV^2 (Ref. 33) is given in Fig. 33. A striking

increase in the relative number of K^+ mesons by a factor of ~2.5 from $Q^2 = 0$ to 1.16 GeV^2 is observed. At $Q^2 = 1.16$ GeV^2 the K^- yield for $p_T \simeq 0$ and Lab. momenta near 2 GeV is approximately equal to that for π^-, while at $Q^2 = 0$ the π^- are more copious by a factor of 10-15. The distribution of the missing mass to K^+, $\gamma_V p \rightarrow K^+ + MM$, suggests (Fig.34, from Ref.33) that most of the K^+ at $Q^2 = 1.16$ GeV^2 and large x come from two-body processes such as $\gamma_V p \rightarrow K^+(\frac{\Lambda}{\Sigma})$, $K^+ Y^*_{1385}$ etc.

The observed increase in K^+ yield appears to be in line with a prediction by K. Wilson[35]; however, the fact that the K^+ stem mostly from two-body reactions seems to indicate that the production process is different from the mechanism Wilson has considered.

d) Proton spectra

The yield of backward going protons ($x < 0$) is displayed in Fig. 35. The peak at $x \approx -0.8$ and $Q^2 = 0$ stems from ρ^o and ω production ($\gamma p \rightarrow p\rho, p\omega$) and disappears with increasing Q^2.

There is considerable interest in the forward proton ($p_T \approx 0$) production at large Q^2. In the parton model of Drell, Levy and Yan[36] one expects the virtual photon at large Q^2 to knock out spin 1/2 partons thus leading e.g. to an excess of forward going protons. In Fig. 36 two DESY measurements at the same W, p_T but $Q^2 = 0$ and $Q^2 = 1.16$ GeV^2 are compared. The electroproduction points in the large x region are lower by 20-30 % and the predicted increase in the number of fast forward going protons is not observed.

Conclusions

1. There is compelling for a new vectorstate, the ρ', with mass near 1.5 GeV and 0.4 - 0.6 GeV width. The inclusion of the ρ' in the VDM-sum rule relating Compton scattering and photoproduction of vector mesons reduces the existing discrepancy from 30 % to 20 % in the amplitude; still further vector mesons are needed to obtain agreement.

2. The relative contribution of the rho electroproduction to the total inelastic cross section decreases at $W \simeq 2.3$ GeV from 16 ± 0.5 % at $Q^2 = 0$ to 4 ± 2 % at $Q^2 = 1.2$ GeV^2. Part of this decreases is due to the t_{min} cut-off.

3. The t distribution for events in the ρ region becomes flatter with increasing Q^2.

4. A substantial fraction of electroproduced rho mesons are longitudinally aligned. The density matrix for events in the ρ region is consistent with SCHC.

5. A 10-20 % decrease in the average number of charged hadrons is observed between $Q^2 = 0$ and 1 GeV^2.

6. No Q^2 variation was found for the π^- spectrum for $x < 0$.

7. The p_T^2 distributions for π^+ and π^- in the photon fragmentation region ($x > 0.4$) become wider with increasing Q^2.

8. The π^+/π^- ratio in the forward direction increases with Q^2.

9. The main features of the Q^2 dependence observed for π^+ and π^- spectra can be understood in terms of two body channels, namely ρ^o production and $\gamma_V p \to \pi^+ n$, $\pi^+ \Delta^o$, $\pi^+ N^*(1520)$.

10. The K^+ yield in the forward direction increases with Q^2 due to the reactions $\gamma_V p \to K^+ (^{\Lambda}_{\Sigma})$, $K^+ Y^*_{(1385)}$.

11. No excess of fast forward going protons has been observed in electroproduction contrary to a parton model prediction.

Acknowledgements

I am grateful to Dr. D. Schildknecht for numerous discussions.

List of References

1. See
Proceedings 1971 International Symposium on Electron and Photon Interactions at High Energies, Cornell University, ed. by N. Mistry.

2. J. J. Sakurai, Ann. Phys. 11, 1 (1960); M. Gell-Mann and F. Zachariasen, Phys. Rev. 124, 953 (1961); Y. Nambu and J. J. Sakurai, Phys. Rev. Letters 8, 79 (1962); M. Gell-Mann, D. Sharp and W. G. Wagner, Phys. Rev. Letters 8, 261 (1962).

3. See
J. le Francois, op. cit. in Ref.1, p.52.

4. V. L. Auslander et al., Phys. Letters 25B, 433 (1967), Sov. J. Nucl. Phys. 9, 144 (1969).

5. G. Buschhorn et al., Phys. Letters 33B, 241 (1970).

6. See e.g.
G. Wolf, DESY Report 70/64 (1970) and op.cit. in Ref.1, p.189.

7. G. Bacci et al., Phys. Letters 38B, 551 (1972); G. Barbarino et al., Lettre al Nuovo Cimento 3, 689 (1972).

8. G. Smadja et al., Lawrence Radiation Laboratory Report LBL-991 (1972); H. H. Bingham et al., SLAC-PUB-1113 and LBL-1085 (1972).

9. M. Davier et al., SLAC-PUB-666 (1969) and contribution to the conference cited in Ref.1.

10. Results reported by Silvestrini at the XVI International Conference on High Energy Physics, Chicago, 1972.

11. SLAC-Berkeley-Tufts Collaboration, Phys. Rev. Letters 24, 960 (1970); Phys. Rev. D5, 545 (1972).

12. SLAC-Berkeley Collaboration, SLAC-PUB (1972).

13. C. Berger et al., Phys. Letters 39B, 659 (1972); R. L. Anderson et al., SLAC-PUB-1085 (1972).

14. L. Hand, Phys. Rev. 129, 1834 (1964).

15. E. D. Bloom et al., Phys. Rev. Letters 23, 930 (1969); M. Breidenbach et al., Phys. Rev. Letters 23, 935 (1969); G. Miller et al., Phys. Rev. D5, 528 (1972).

16. W. Albrecht et al., Nucl. Phys. B27, 615 (1971).

17. J. Moritz et al., DESY Report 71/61 (1971);
F. W. Brasse et al., DESY Report 71/2 (1971).

18. V. Eckardt et al., Electroproduction in a Streamer Chamber at 7.2 GeV and $0.3 < Q^2 < 1.5$ GeV^2;
Part I: Experimental Setup, Multiplicities and Inclusive π^- Spectra.
Part II: Study of Δ^{++} and ρ^0 Production in the Reaction $ep \to ep\pi^+\pi^-$.
Papers submitted to the XVI International Conference on High Energy Physics, Chicago, 1972.

19. C. Driver et al., Phys. Letters 35B, 77; 81 (1971);
Nucl. Phys. B30, 245 (1971); B32, 45 (1971); B33, 84 (1971).
C. N. Brown et al., Phys. Rev. Letters 26, 987 (1971);
26, 991 (1971); 27, 536 (1971).
P. S. Kummer et al., Lettre Nuovo Cimento 1, 1026 (1971);
D. Andrews et al., Cornell Report CLNS-169 (1971).

20. K. Berkelman, rapporteur's talk, op. cit. in Ref.1, p. 264.
W. T. Toner, Rutherford Laboratory Report RPP/H/97 (1972).

21. J. Ballam et al., A Study of Hadronic Final States from Inelastic Muon Scattering in a Hybrid Bubble Chamber Experiment. Paper submitted to the XVI International Conference on High Energy Physics, Chicago, 1972.

22. H. Fraas and D. Schildknecht, Nucl. Phys. B14, 543 (1969);
J. J. Sakurai, Phys. Rev. Letters 22, 981 (1969).

23. J. C. Alder et al., DESY Report 72/38 (1972).

24. H. Cheng and T. T. Wu; Phys. Rev. 183, 1324 (1969);
J. D. Bjorken, J. Kogut and D. Soper, Phys. Rev. D1, 1382 (1971);
H. T. Nieh, Phys. Letters B38, 100 (1972).

25. Aachen-Berlin-Bonn-Hamburg-Heidelberg-München Collaboration, Phys. Rev. 175, 1669 (1968), and H. Spitzer, Internal Report DESY F-1 (1971).

26. J. Dakin et al., Phys. Rev. Letters 29, 746 (1972)

27. Ahrens et al., data quoted by K. Berkelmann at the XVI International Conference on High Energy Physics, Chicago, 1972.

28. K. G. Wilson, Acta Phys. Austr. 17, 37 (1963); Cornell Report CLNS-BI (1970);
C. E. De Tar, Phys. Rev. D3, 128 (1971).

29. Aachen-Hamburg-Heidelberg-München Collaboration, contribution to the XVI International Conference on High Energy, Chicago, 1972.

30. I. Dammann et al., ibid.

31. E. Lazarus et al., Phys. Rev. Letters 29, 743 (1972).

32. H. Burfeindt et al., ibid.

33. J. C. Alder et al., DESY Report 72/31 (1972).

34. The ρ^0 contribution to the $\pi^{\mp}$ Yield for $p_T^2 < 0.04$ GeV^2 has been determined by K. C. Moffeit from the data of the SLAC-Berkeley-Tufts Collaboration, Phys. Rev. D5, 1603 (1972).

35. K. Wilson, Triest Preprint, IC/71/47 (1971) and private communication.

36. S. D. Drell, D. J. Levy and T. M. Yan, Phys. Rev. Letters 22, 744 (1969).

Table 1 Properties of the ρ' (Ref. 11)

a) from $e^+e^- \to$ pions

$J^P_{\rho'} = 1^-$, $I^G = 1^+$

$M_{\rho'} \cong 1.6$ GeV* $\quad \Gamma_{\rho'} \cong 0.3 - 0.4$ GeV*

$$\frac{\rho' \to 2\pi^+ 2\pi^-}{\rho' \to \text{all}} \cong 0.5 - 0.7$$

$$(\gamma_{\rho'}/\gamma_\rho)^2) \simeq 4$$

b) from photoproduction at $E_\gamma = 9.3$ GeV (Ref. 8)

$J^P_{\rho'} = ?$, $I^G = 1^+$

$M_{\rho'} = 1.43 \pm 0.05$ GeV $\quad \Gamma_{\rho'} = 0.65 \pm 0.1$ GeV**

observed decay mode: $\rho' \to \rho^o\sigma \to 2\pi^+ 2\pi^-$

$$\frac{\rho' \to \pi^+\pi^-}{\rho' \to \rho^o\pi^+\pi^-} < 0.2 \; ; \quad \frac{\rho' \to K^+K^-}{\rho' \to \rho^o\pi^+\pi^-} < 0.04 \qquad (90\%\ \text{C.L.})$$

$\sigma(\gamma p \to p\rho'_{\hookrightarrow \rho^o\sigma})$*** $= 2.4 \pm 0.6$ μb

$d\sigma/dt(\gamma p \to p\rho' \to \rho^o\sigma) \simeq (15 \pm 4)\ (\mu b/\text{GeV}^2)\ e^{(5.6 \pm 0.3)t}$

$(\gamma_{\rho'}/\gamma_\rho)^2 \simeq 6 \pm 2$ if ρ' decays only into $\rho^o\sigma$.

---

* numbers are from an eyeball fit (Ref. 10).

** numbers come from Maximumlikelihood fit; are sensitive to energy dependence of $\Gamma_{\rho'}$ (Ref. 8).

*** corrected by factor $\frac{3}{2}$ for decay $\rho^o\sigma \to \rho^o\pi^o\pi^o$.

Table 2 Input values for the Compton sum rule (Eq(2)).

	V = ρ	ω	φ	ρ'
$\gamma_V^2/4\pi$	0.64±0.05 [3]	4.8±0.5 [3]	2.8 ±0.2 [3]	3.9±1.3
$d\sigma^o/dt(\gamma p \to Vp)$ $(\mu b/GeV^2)$	100 ±15 [6]	11.2±2.1 [12]	2.85±0.2 [13]	15 ±5

Table 3 Reaction $ep \to ep\rho^o$:
Ratio of ρ^o to total cross section at $2 < W < 2.7$ GeV.
Data taken from Ref. 11 ($Q^2 = 0$) and Ref. 18.

Q^2 (GeV^2)	σ_ρ/σ_{tot}
0	16 ± 0.5 %
0.4	9 ± 2 %
0.65	7 ± 2 %
1.1	4 ± 2 %

Table 4 Exponential Fit, $d\sigma/dt = d\sigma^o/dt \exp(At)$ to ρ^o-electroproduction, taking all events in the ρ region

Experiment	W (GeV)	Q^2 (GeV^2)	t-Range (GeV^2)	$d\sigma^o/dt$ ($\mu b/GeV^2$)	A (GeV^{-2})
SBT[11] $\gamma p \to p\pi^+\pi^-$	2.48	0	<1.0	148±6.7	6.2±0.2
DESY-STC[18] $ep \to ep\pi^+\pi^-$	2-2.7	0.3 -0.5	<1.0	32±11	4.1±1.0
		0.5 -0.8	<1.0	15±6.5	3.2±1.0
SLAC-HBC[21] $\mu p \to \mu p\pi^+\pi^-$	2-4	0.15-0.5	0.05-0.6		7.2±2.1
		0.5 -2	0.05-0.6		5.1±1.2
Cornell[27] $ep \to epMM$	~3	0.6	<0.8		4.3
		1.1	<0.8		2.9

Table 5 ρ-density matrix elements in the helicity system from events of the reaction $ep \to ep\pi^+\pi^-$ in the ρ region ($0.65 < M_{\pi^+\pi^-} < 0.84$ GeV). (From Ref. 18).

	$2<W<2.7$ GeV $Q^2=0.60$ GeV^2	Prediction from SCHC with R = 0.6
r^{04}_{00}	0.35 ± 0.07	0.35
Re r^{04}_{10}	0.08 ± 0.05	0
r^{04}_{1-1}	-0.09 ± 0.07	0
r^{1}_{00}	-0.04 ± 0.11	0
r^{1}_{11}	-0.08 ± 0.07	0
Re r^{1}_{10}	-0.03 ± 0.07	0
r^{1}_{1-1}	0.26 ± 0.10	0.32
Im r^{2}_{10}	-0.04 ± 0.07	0
Im r^{2}_{1-1}	-0.27 ± 0.11	-0.32
r^{5}_{00}	-0.05 ± 0.06	0
r^{5}_{11}	-0.02 ± 0.04	0
Re r^{5}_{10}	0.00 ± 0.04	$0.18\ \cos\delta$*
r^{5}_{1-1}	0.10 ± 0.06	0
Im r^{6}_{10}	-0.02 ± 0.04	$-0.18\ \cos\delta$*
Im r^{6}_{1-1}	0.04 ± 0.05	0

* δ = phase between production by longitudinal and transverse photons

Figure Captions

1. Cross section for $e^+e^- \to 2\pi^+2\pi^-$. Fig. taken from Ref. 10.

2. Reaction $\gamma p \to p2\pi^+2\pi^-$ at 9.3 GeV:
   (a) Four pion mass spectrum. The shaded histogram has events with Δ^{++} removed ($M_{p\pi^+} > 1.32$ GeV).
   (b) π^+p mass distribution. The shaded events have $M_{4\pi} < 1.7$ GeV. The curve is from a Maximum-Likelihood fit.
   (c) $\pi^+\pi^-$ mass distribution ($M_{4\pi} < 1.7$ GeV) for $\pi^+\pi^-$ pairs opposite a ρ^o. The dotted (solid) curve shows the distribution expected for $\rho^o\rho^o$ ($\rho^o\pi^+\pi^-$ + phase space).
   (d) $\pi^+\pi^-$ mass distribution. The shaded events are for $M_{4\pi} < 1.7$ GeV. The curve is from a Maximum-Likelihood fit.
   Fig. taken from Ref. 8.

3. Reaction $\gamma p \to p2\pi^+2\pi^-$ at 9.3 GeV:
   Distribution of the angles Θ and ψ for $M_{4\pi} < 1.7$ GeV.
   The curves are from a Maximum-Likelihood fit.
   Fig. taken from Ref.8.

4. Total electroproduction cross section, $\sigma_T^{Tot} + \varepsilon\sigma_L^{Tot}$, as a function of Q^2 for various W(W = effective mass of the outgoing hadron system). Data from Refs. 15,17,18. Fig. taken from Ref. 18.

5. Layout of the DESY streamer chamber experiment to study electroproduction. Fig. taken from Ref. 18.

6. Photograph from the DESY streamer chamber experiment. The label e marks the electron beam. About 50-100 beam electrons have passed the chamber during the memory time. The label e' marks the scattered electron.

7. Layout of the SLAC bubble chamber experiment to study inelastic μp scattering. Fig. taken from Ref. 21.

8. Total cross section for the reaction $ep \to ep\pi^+\pi^-$ as a function of the total hadron effective mass W for different Q^2 intervals (Ref.18). Also shown is the total cross section for $\gamma p \to p\pi^+\pi^-$ from the ABBHHM collaboration[25]. Fig. taken from Ref. 18.

9. Reaction $ep \to ep\pi^+\pi^-$: Q^2 dependence of the cross section for different W intervals (Ref.18). The $Q^2 = 0$ points are from Ref. 25. Fig. taken from Ref. 18.

10. Reaction $ep \to ep\pi^+\pi^-$: $p\pi^+$ mass distributions. Fig. taken from Ref. 18.

11. Reaction $ep \to ep\pi^+\pi^-$: $p\pi^+$ and $\pi^+\pi^-$ mass distributions. Fig. taken from Ref. 18.

12. Reaction $ep \to ep\pi^+\pi^-$: $p\pi^+$ and $\pi^+\pi^-$ mass distributions. Fig. taken from Ref. 18.

13. Reaction $\mu p \to \mu p\pi^+\pi^-$: $\pi^+\pi^-$ mass distribution for $0.15 < Q^2 < 3$ GeV^2 and $2 < W < 4$ GeV. Fig. taken from Ref.21.

14. Reaction $ep \to ep\pi^+\pi^-$: $\pi^+\pi^-$ mass distribution. Fig. taken from Ref.26.

15. Reaction $ep \to ep$ + missing mass for $W \approx 3$ GeV. Fig. taken from Ref. 27.

16. Reaction $ep \to ep\rho^o$. Total cross section as a function of Q^2 for different W intervals (⧫). The open points, ◊, show the cross section data when multiplied by $e^{A|t|_{min}}$ to account for the $|t|_{min}$ cutoff. The values at $Q^2 = 0$ have been measured by the ABBHHM Collaboration[25]. The dashed-dotted curves show the Q^2 dependence of the total inelastic ep cross section normalized to the cross section point at $Q^2 = 0$. Fig. taken from Ref. 18.

17. Reaction $ep \to ep\pi^+\pi^-$: Differential cross section, $d\sigma/dt$, for events in the ρ region (⧫). The cross sections have been normalized to the total ρ cross section. The open points (◊) show the photoproduction data[11] treated in the same manner. Fig. taken from Ref. 18.

18. Reaction $\mu p \to \mu p\pi^+\pi^-$: t distribution for events in the ρ region. Fig. taken from Ref. 21.

19. Slope values for photo- and electroproduction of $p\pi^+\pi^-$ events in the rho region as a function of $\Delta\tau = \frac{2\nu}{Q^2+m_\rho^2}$. The photoproduction points are those of Cornell, SLAC-WSC, the SLAC-Berkeley-Tufts Collaboration and the SLAC-Weizmann-Tel-Aviv Collaboration as quoted in Ref. 6. The electroproduction points stem from Ref. 18 (⧫) and Ref. 24 (▲).

20. Reaction $ep \to ep\rho^o$: Definition of decay angles Θ_H, ψ_H in the helicity system for forward ρ^o production.

21. Reaction $\gamma p \to p\pi^+\pi^-$: Decay angular distributions in the helicity system for events in the ρ region.
Fig. taken from Ref. 11.

22. Reaction $ep \to ep\pi^+\pi^-$: Decay angular distributions in the helicity system for all events in the ρ region. Fig. taken from Ref. 18.

23. Reaction $\mu p \to \mu p\pi^+\pi^-$. Decay angular distributions in the helicity system for events in the ρ region. Fig. taken from Ref. 21.

24. Reaction $\mu p \to \mu p\pi^+\pi^-\pi^o$:
(a) $\pi^+\pi^-\pi^o$ mass distribution
(b) cross section for $\mu p \to \mu p\omega$
Fig. taken from Ref. 21.

25. Average hadron multiplicity in $ep \to e$ + hadrons and $\mu p \to \mu$ + hadrons for different W intervals. Data from Refs. 18, 21.

26. Invariant cross section $f = E\frac{d^3\sigma}{dp^3}$ as a function of p_T^2 for different x and Q^2 intervals. Data from Refs. 29,30. The straight lines have been calculated for different values of the exponential slope A. Fig. taken from Ref. 30.

27. π^+ yield as a function of p_T^2 in the central region. Fig. taken from Ref. 31.

28. The normalized π^- yield for $ep \to e\pi^-$ + ... at W = 2.6 GeV and $Q^2 = 0$ (Ref. 29), and at $2.0 < W < 2.7$ GeV for different Q^2 intervals (Ref. 18). The curves show the π^- yield at $Q^2 = 0$ when ρ^o events from $\gamma p \to p\rho^o$ are removed.
Fig. taken from Ref. 18.

29. The normalized invariant cross section for $\gamma p \to \pi^- x$ and $ep \to e\pi^- x$ for $p_T^2 \lesssim 0.02$ GeV^2 at W = 2.63 GeV, $Q^2 = 0$ (Ref.32) and $Q^2 = 1.16$ GeV^2 (Ref. 33). The curve shows the π^- cross section at $Q^2 = 0$ after ρ^o events from $\gamma p \to p\rho^o$ have been removed.[34]

30. The normalized invariant cross section for $\gamma p \to \pi^+ x$ and $ep \to e\pi^+ x$ for $p_T^2 < 0.02$ GeV^2 at W = 2.63 GeV, $Q^2 = 0$ (Ref.32) and $Q^2 = 1.16$ GeV^2 (Ref.33). The curve shows the π^+ cross section at $Q^2 = 0$ after ρ^o events from $\gamma p \to p\rho^o$ have been removed.[34]

31. Missing mass spectrum for inclusive $\pi^\pm$ electroproduction at $p_T^2 < 0.02$ GeV^2, W = 2.63 GeV and $Q^2 = 1.16$ GeV^2. Fig. taken from Ref. 33.

32. Normalized invariant cross sections for inclusive production as a function of Q^2 for different x intervals. Data stem from Refs. 30,32,33. Fig. taken from Ref. 30.

33. The normalized invariant cross sections for inclusive K^+ production at $p_T^2 < 0.02$ GeV^2, W = 2.63 GeV, $Q^2 = 0$ (Ref.32) and $Q^2 = 1.16$ GeV^2 (Ref.33). Fig. taken from Ref. 32.

34. Missing mass spectrum for inclusive K^+ production at $p_T^2 < 0.02$ GeV^2, W = 2.63 GeV and $Q^2 = 1.16$ GeV. Fig. taken from Ref. 33.

35. The normalized invariant cross sections for inclusive proton production for $x < -0.5$. Fig. taken from Ref. 21.

36. The normalized invariant cross sections for inclusive proton production at $p_T^2 < 0.02$ GeV^2, W = 2.63 GeV, $Q^2 = 0$ (Ref.32) and $Q^2 = 1.16$ GeV^2 (Ref.33). Fig. taken from Ref. 32.

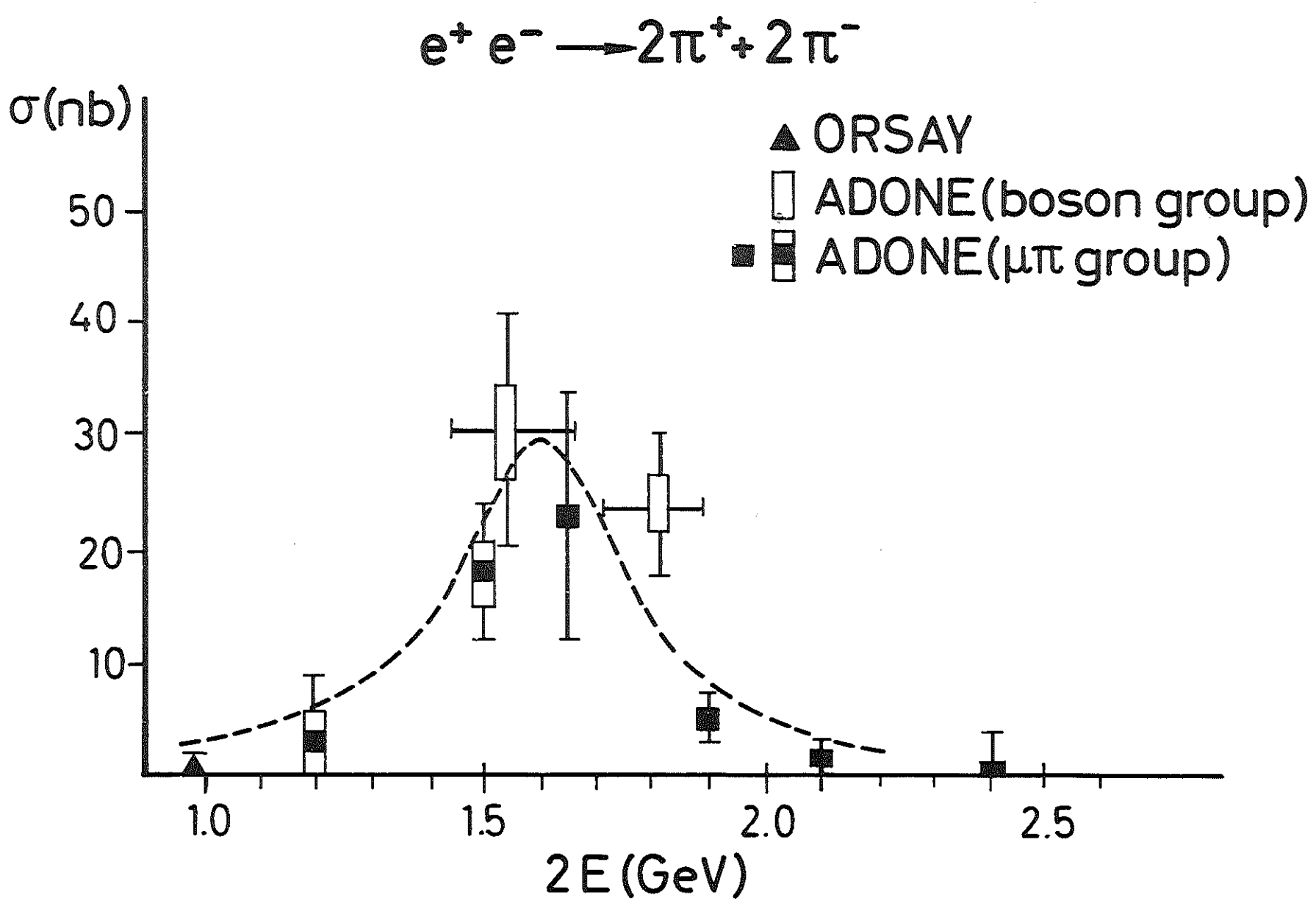
$e^+ e^- \longrightarrow 2\pi^+ + 2\pi^-$
σ(nb)
50
40
30
20
10
ORSAY
ADONE(boson group)
ADONE(μπ group)
1.0
1.5
2.0
2.5
2E(GeV)

Fig. 1

SLAC-LBL-TUFTS

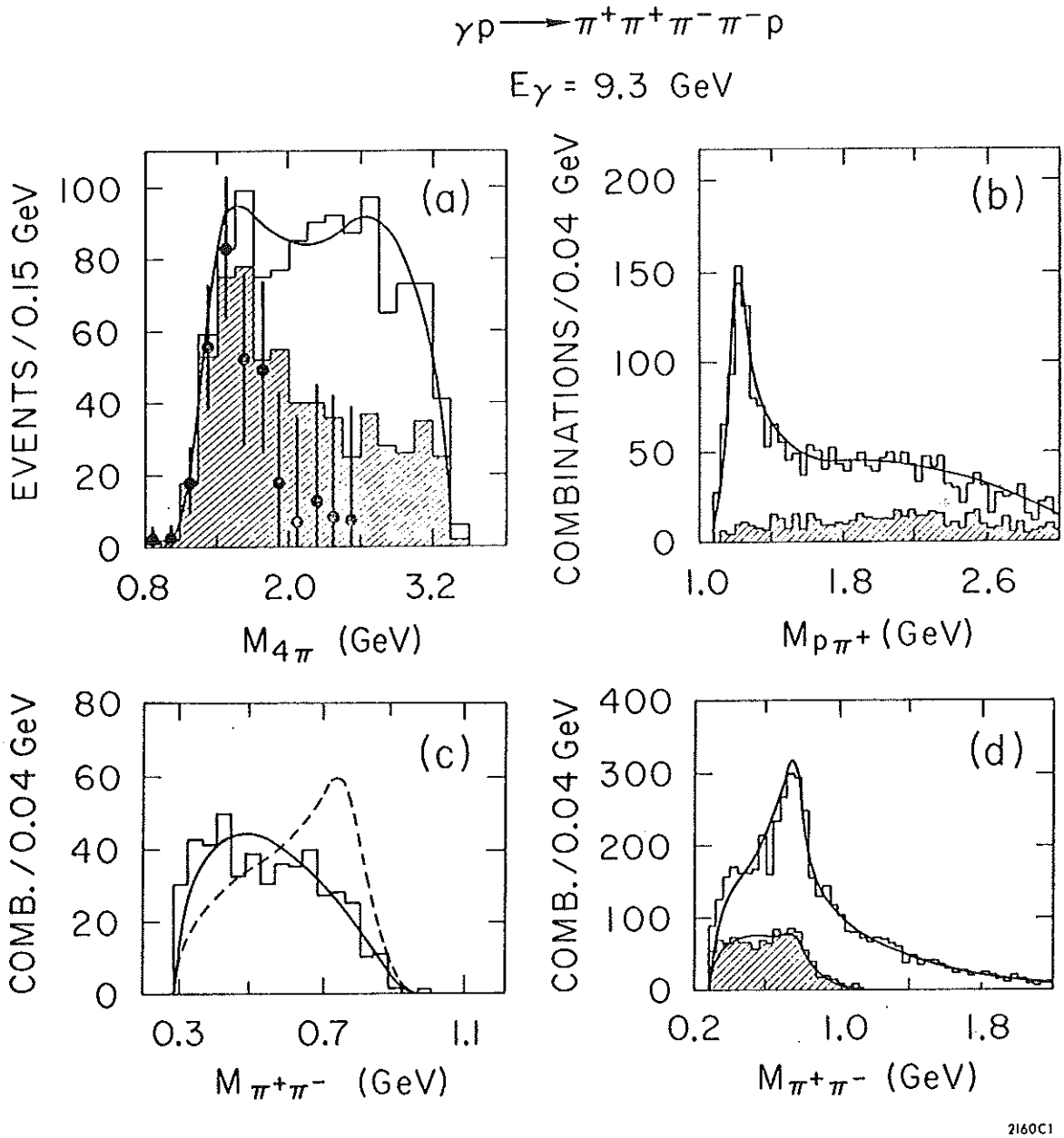

Fig. 2

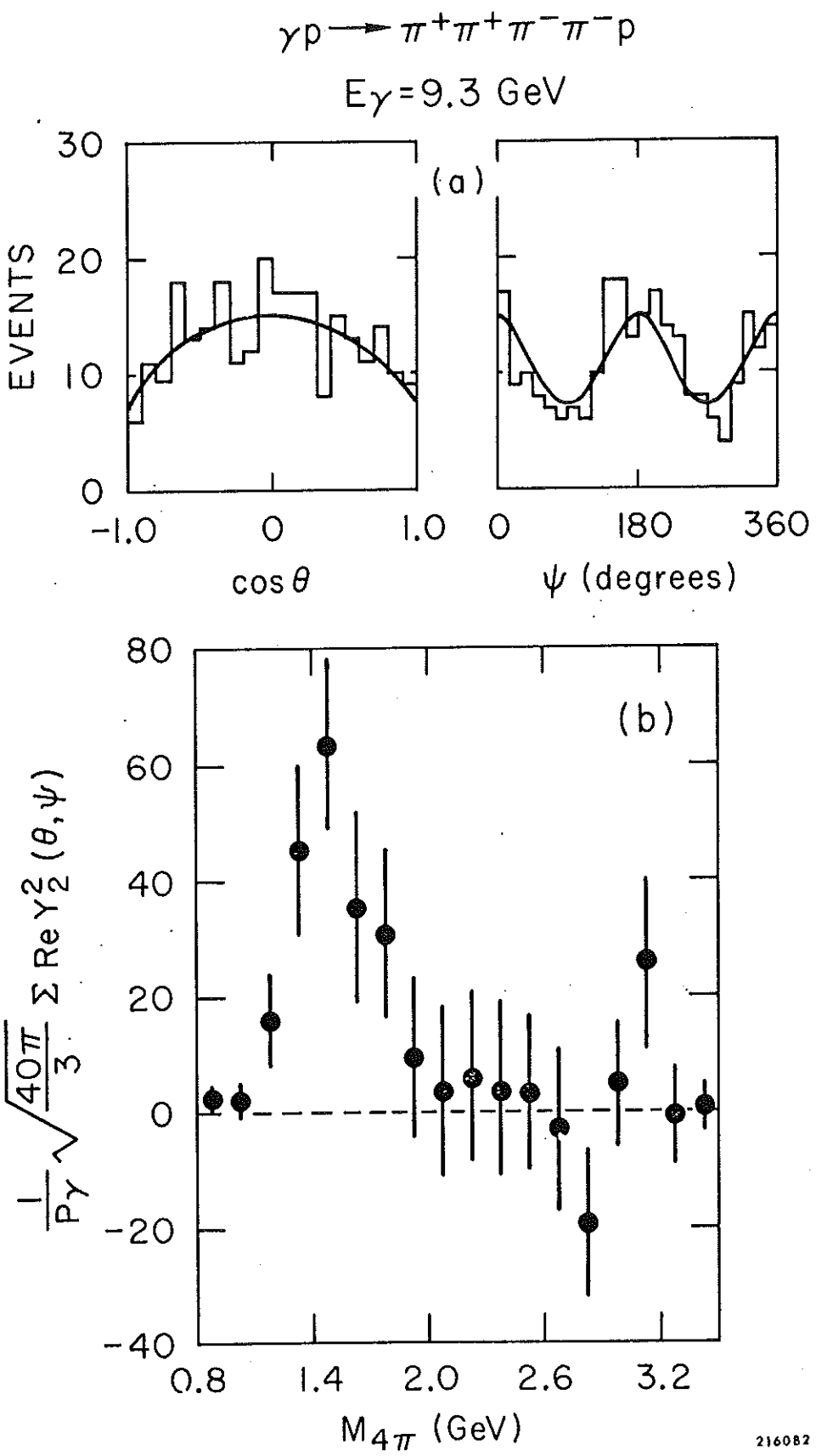
SLAC-LBL-TUFTS
γp → π+π+π−π−p
Eγ = 9.3 GeV
(a)
EVENTS
30
20
10
0
-1.0
0
1.0
cos θ
0
180
360
ψ (degrees)
(b)
80
60
40
20
0
-20
-40
0.8
1.4
2.0
2.6
3.2
M4π (GeV)
1/Pγ √(40π/3) Σ Re Y2^2 (θ,ψ)
216082

Fig. 3

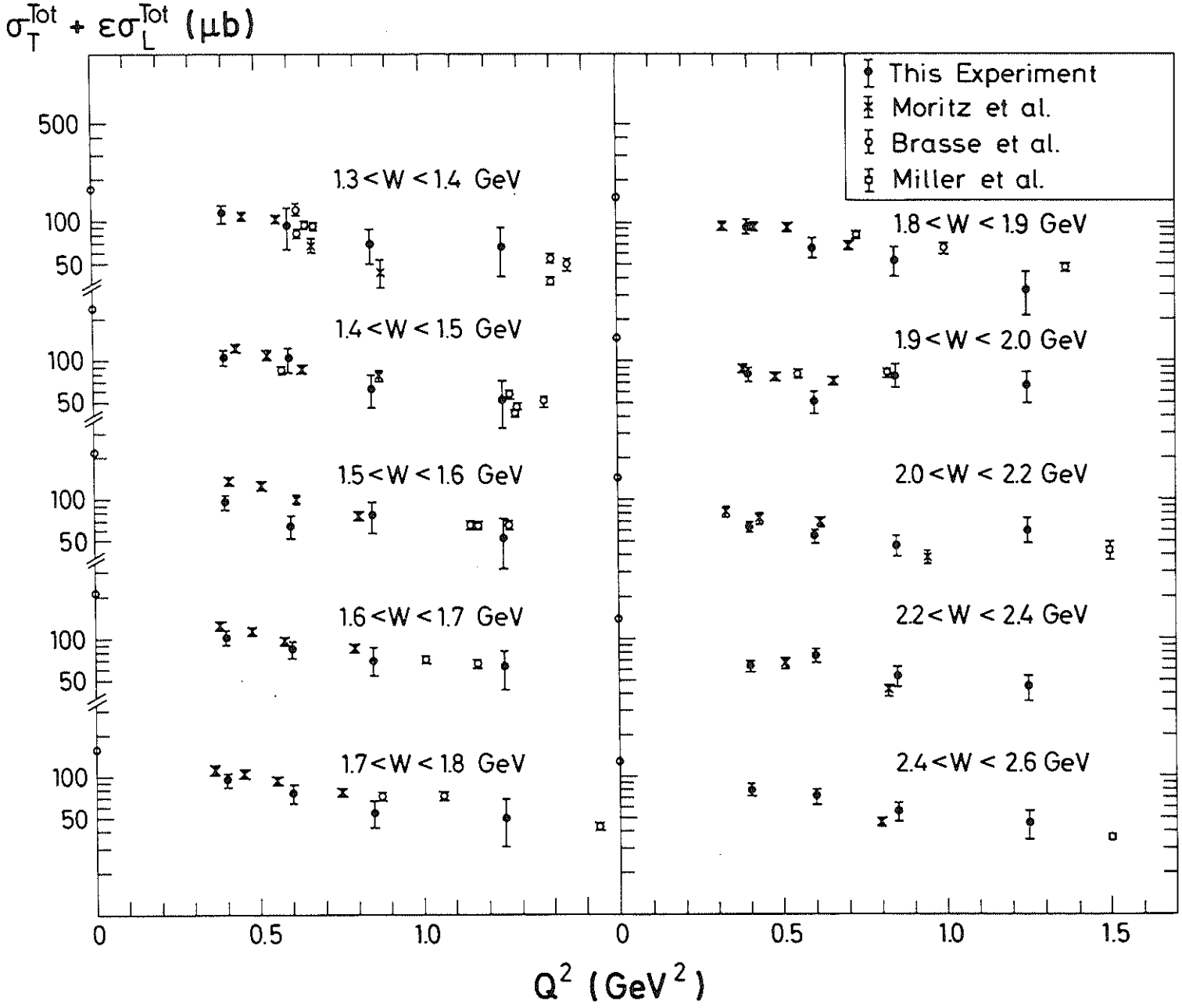
$\sigma_T^{Tot} + \varepsilon\sigma_L^{Tot}$ (μb)
This Experiment
Moritz et al.
Brasse et al.
Miller et al.
1.3 < W < 1.4 GeV
1.4 < W < 1.5 GeV
1.5 < W < 1.6 GeV
1.6 < W < 1.7 GeV
1.7 < W < 1.8 GeV
1.8 < W < 1.9 GeV
1.9 < W < 2.0 GeV
2.0 < W < 2.2 GeV
2.2 < W < 2.4 GeV
2.4 < W < 2.6 GeV
500
100
50
0
0.5
1.0
1.5
Q^2 (GeV^2)

Fig. 4

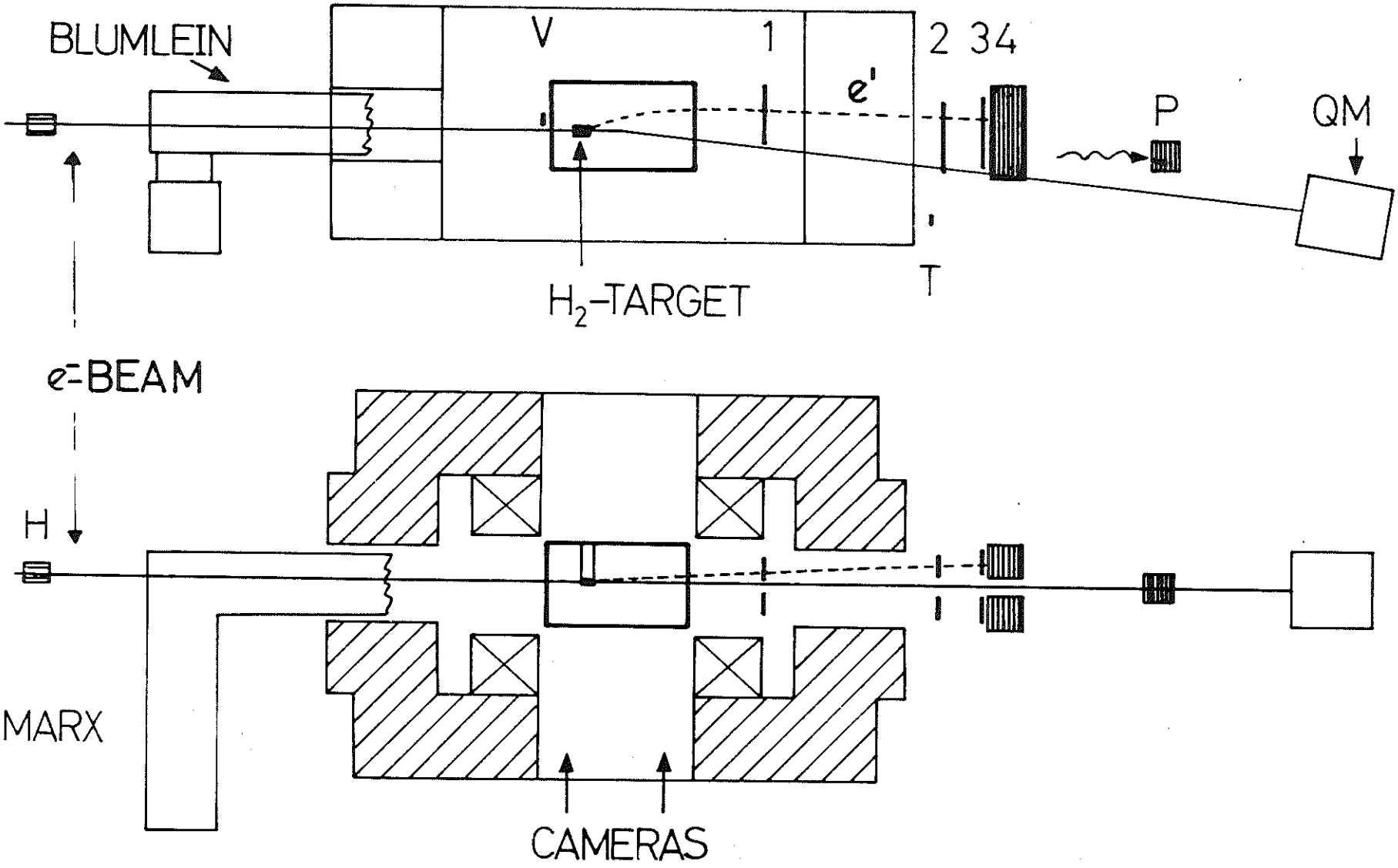

Fig. 5

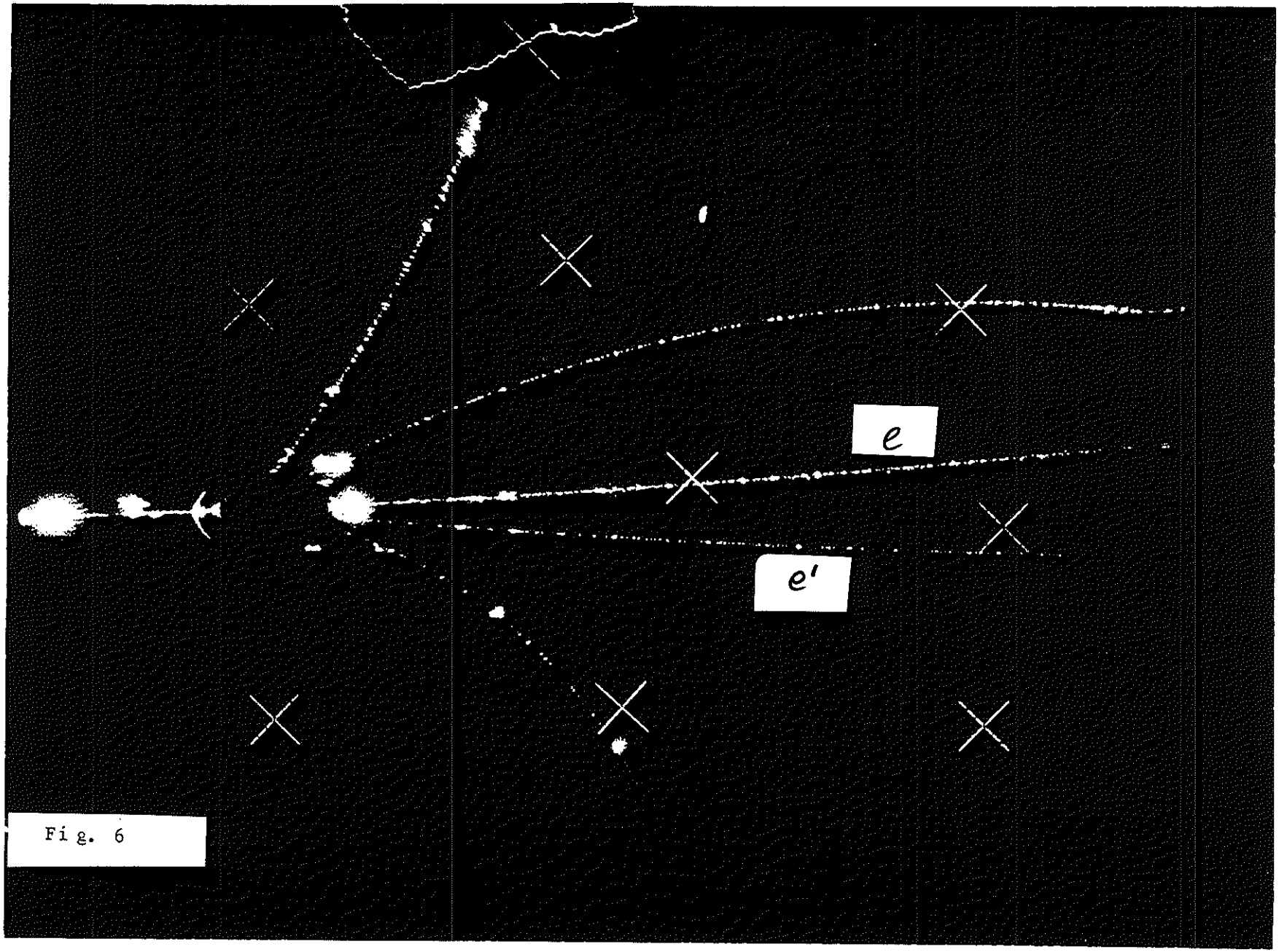

Fig. 6

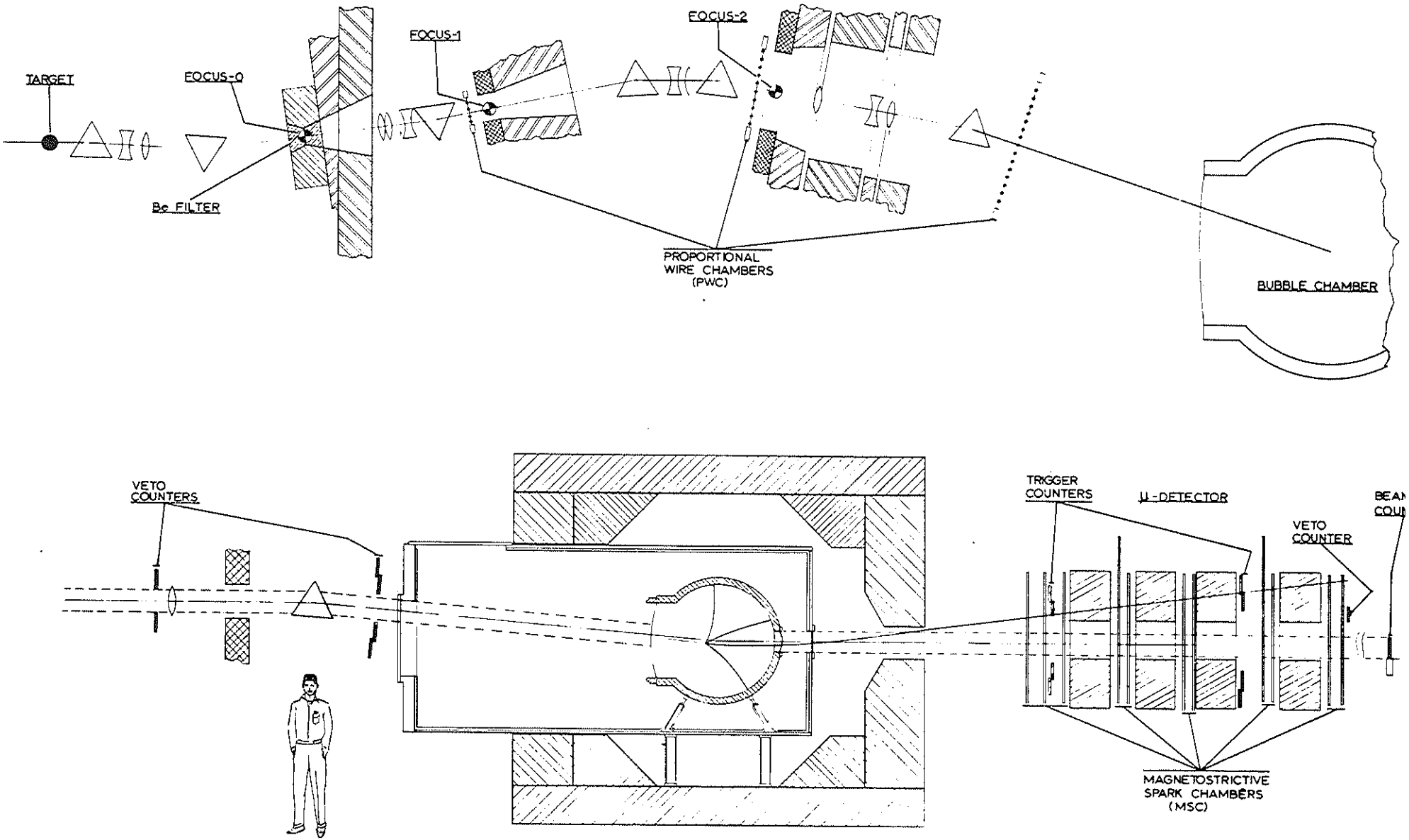
TARGET
FOCUS-0
Be FILTER
FOCUS-1
FOCUS-2
PROPORTIONAL
WIRE CHAMBERS
(PWC)
BUBBLE CHAMBER
VETO
COUNTERS
TRIGGER
COUNTERS
μ-DETECTOR
VETO
COUNTER
MAGNETOSTRICTIVE
SPARK CHAMBERS
(MSC)

Fig. 7

DESY

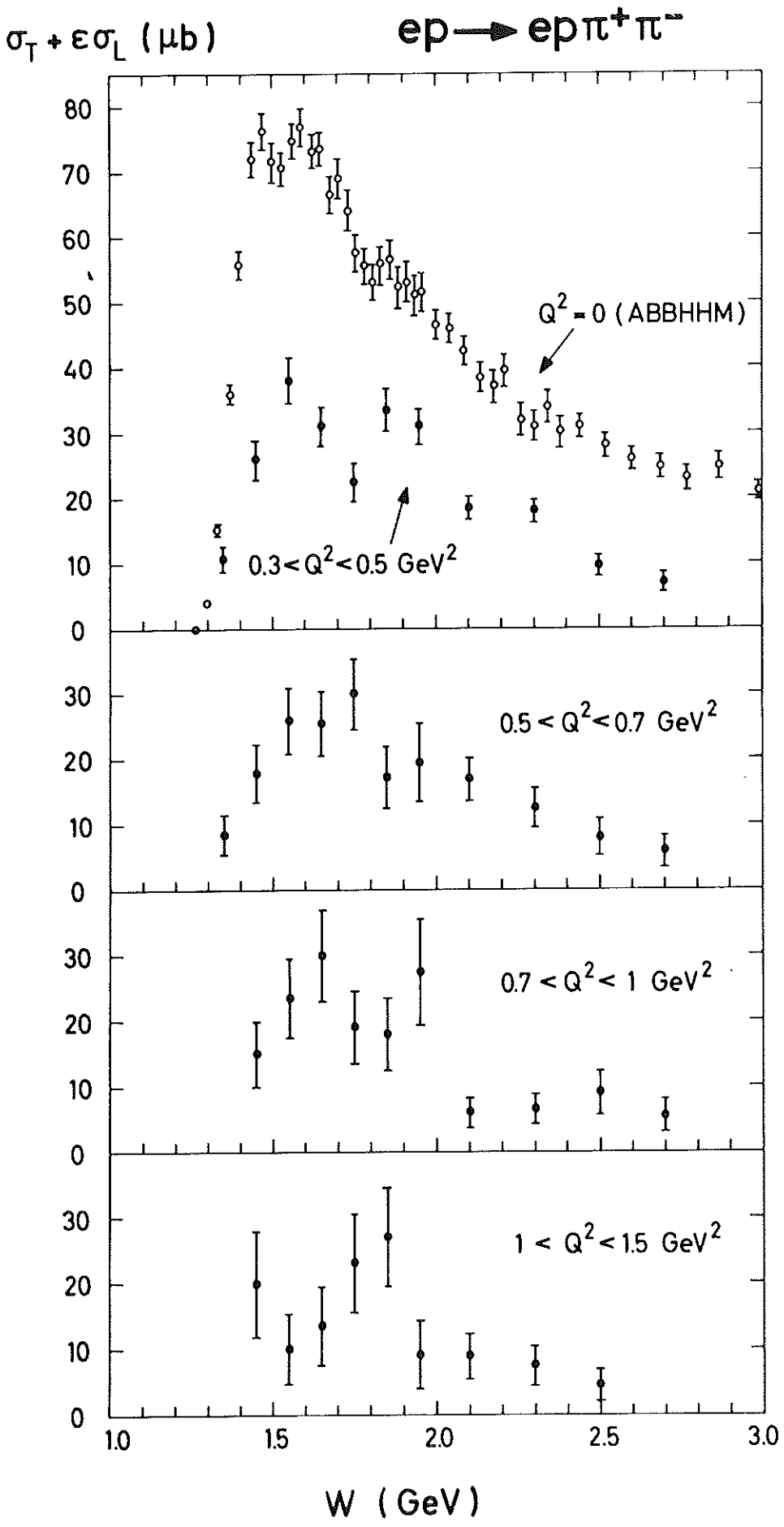
$\sigma_T + \varepsilon\sigma_L$ (μb)
$ep \rightarrow ep\pi^+\pi^-$
$Q^2 = 0$ (ABBHHM)
$0.3 < Q^2 < 0.5$ GeV^2
$0.5 < Q^2 < 0.7$ GeV^2
$0.7 < Q^2 < 1$ GeV^2
$1 < Q^2 < 1.5$ GeV^2
W (GeV)

Fig. 8

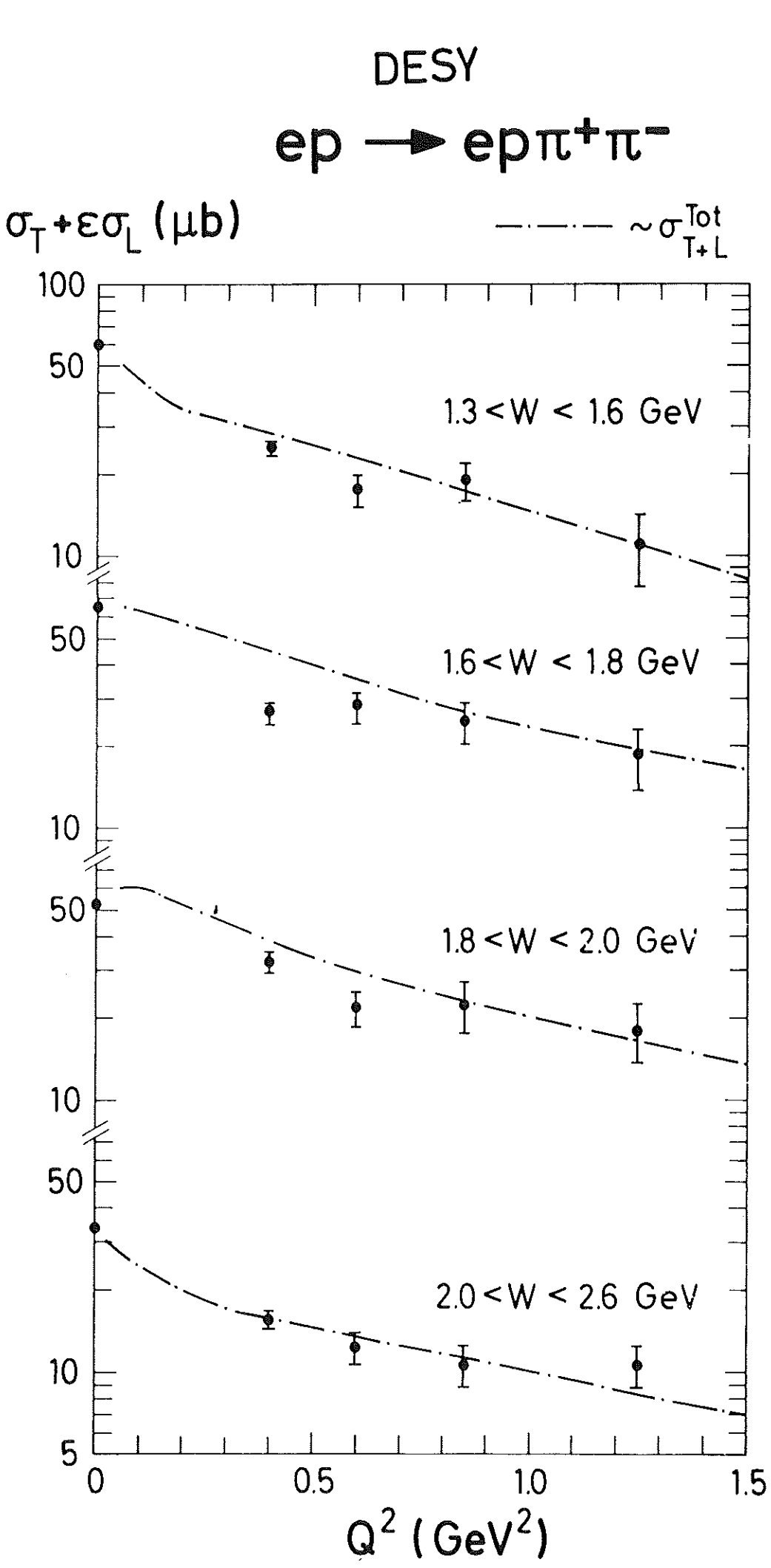
DESY
ep → epπ+π−
σT+εσL (μb)
— · — · — ~σTot T+L
100
50
10
50
10
50
10
50
10
5
1.3 < W < 1.6 GeV
1.6 < W < 1.8 GeV
1.8 < W < 2.0 GeV
2.0 < W < 2.6 GeV
0
0.5
1.0
1.5
Q2 (GeV2)

Fig. 9

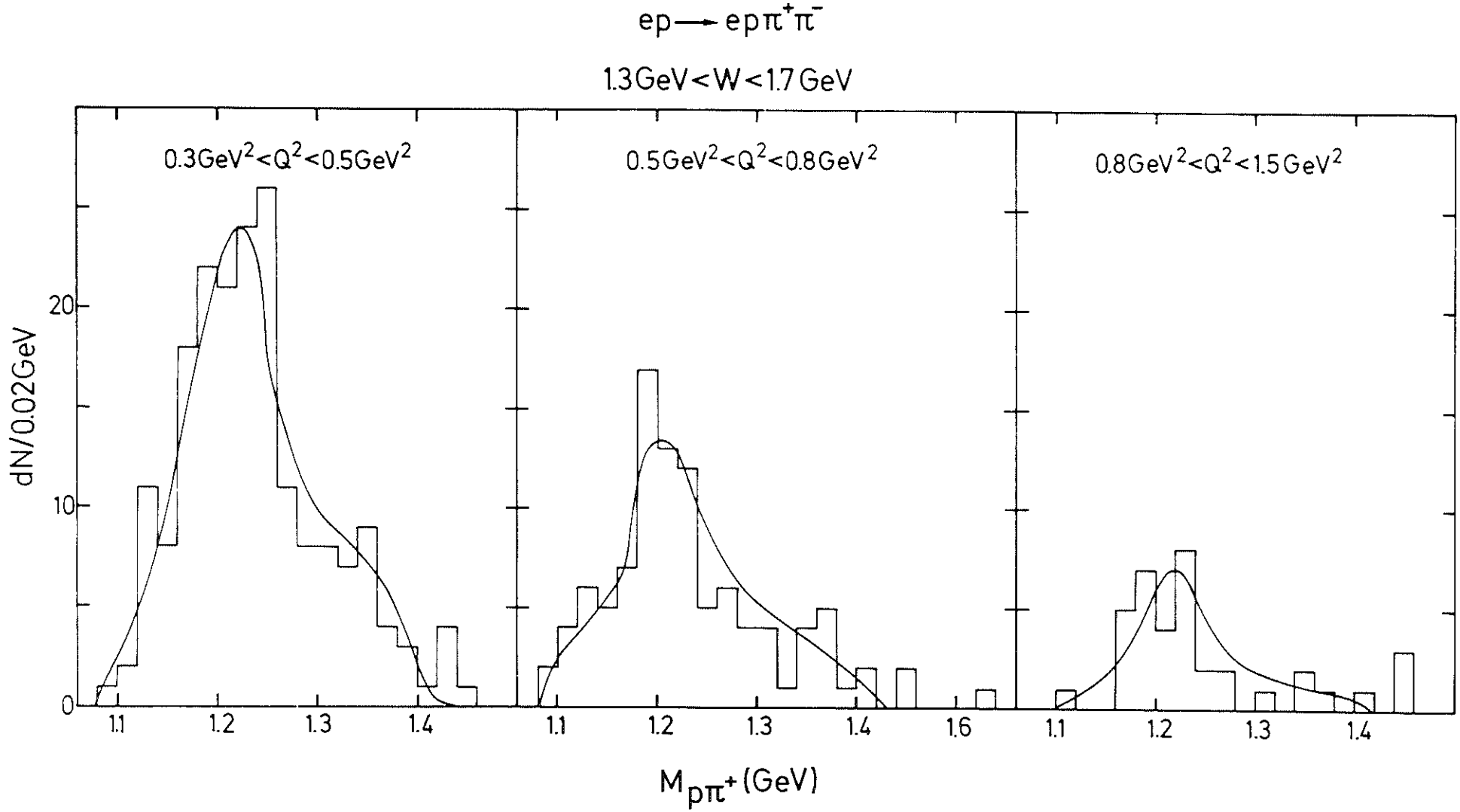
ep → epπ⁺π⁻
1.3GeV<W<1.7 GeV
0.3GeV²<Q²<0.5GeV²
0.5GeV²<Q²<0.8GeV²
0.8GeV²<Q²<1.5GeV²
dN/0.02GeV
0
10
20
1.1
1.2
1.3
1.4
1.6
Mpπ⁺ (GeV)

Fig. 10

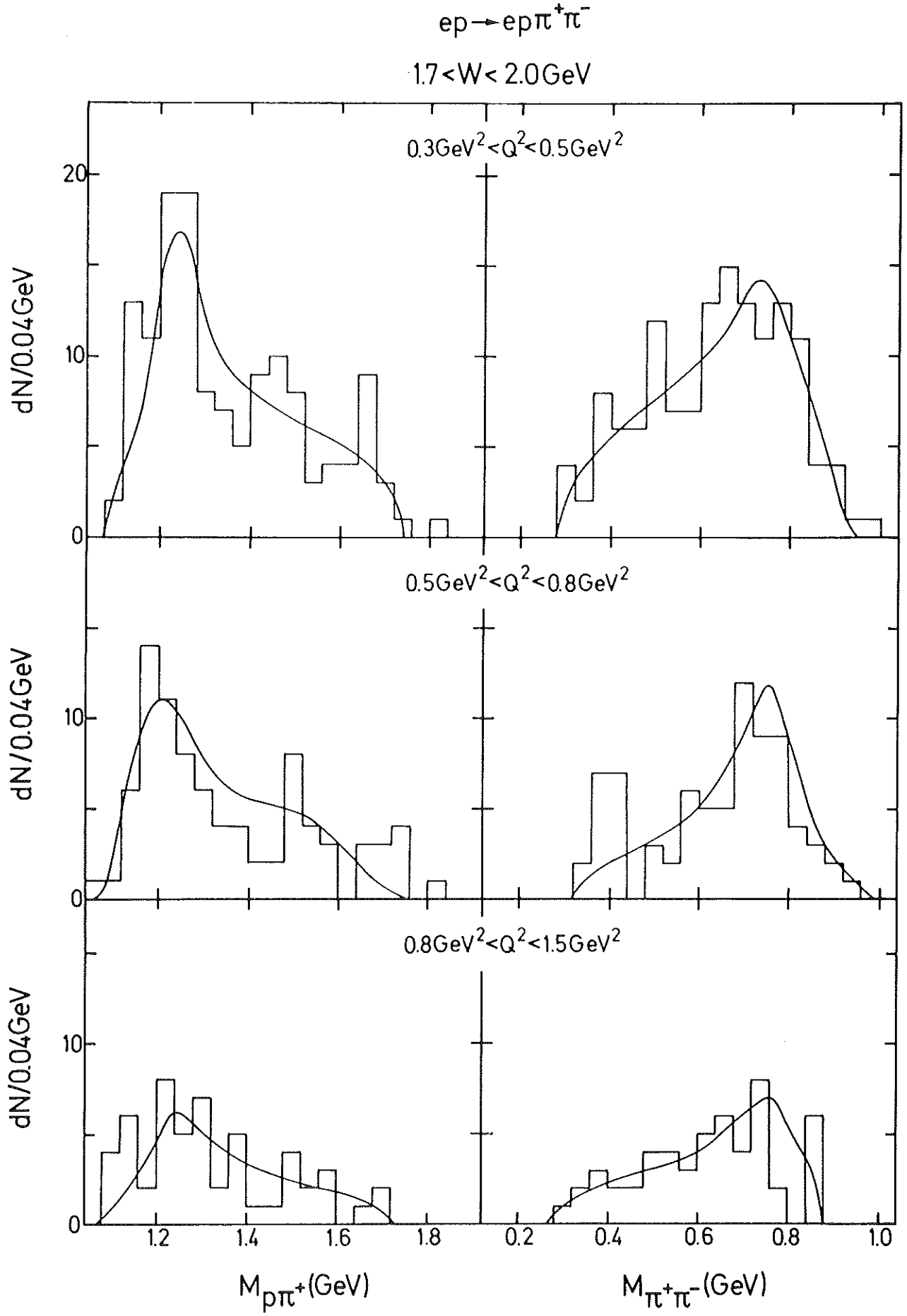
ep→epπ⁺π⁻
1.7<W<2.0GeV
0.3GeV²<Q²<0.5GeV²
0.5GeV²<Q²<0.8GeV²
0.8GeV²<Q²<1.5GeV²
dN/0.04GeV
20
10
0
1.2
1.4
1.6
1.8
0.2
0.4
0.6
0.8
1.0
Mpπ⁺(GeV)
Mπ⁺π⁻(GeV)

Fig. 11

DESY

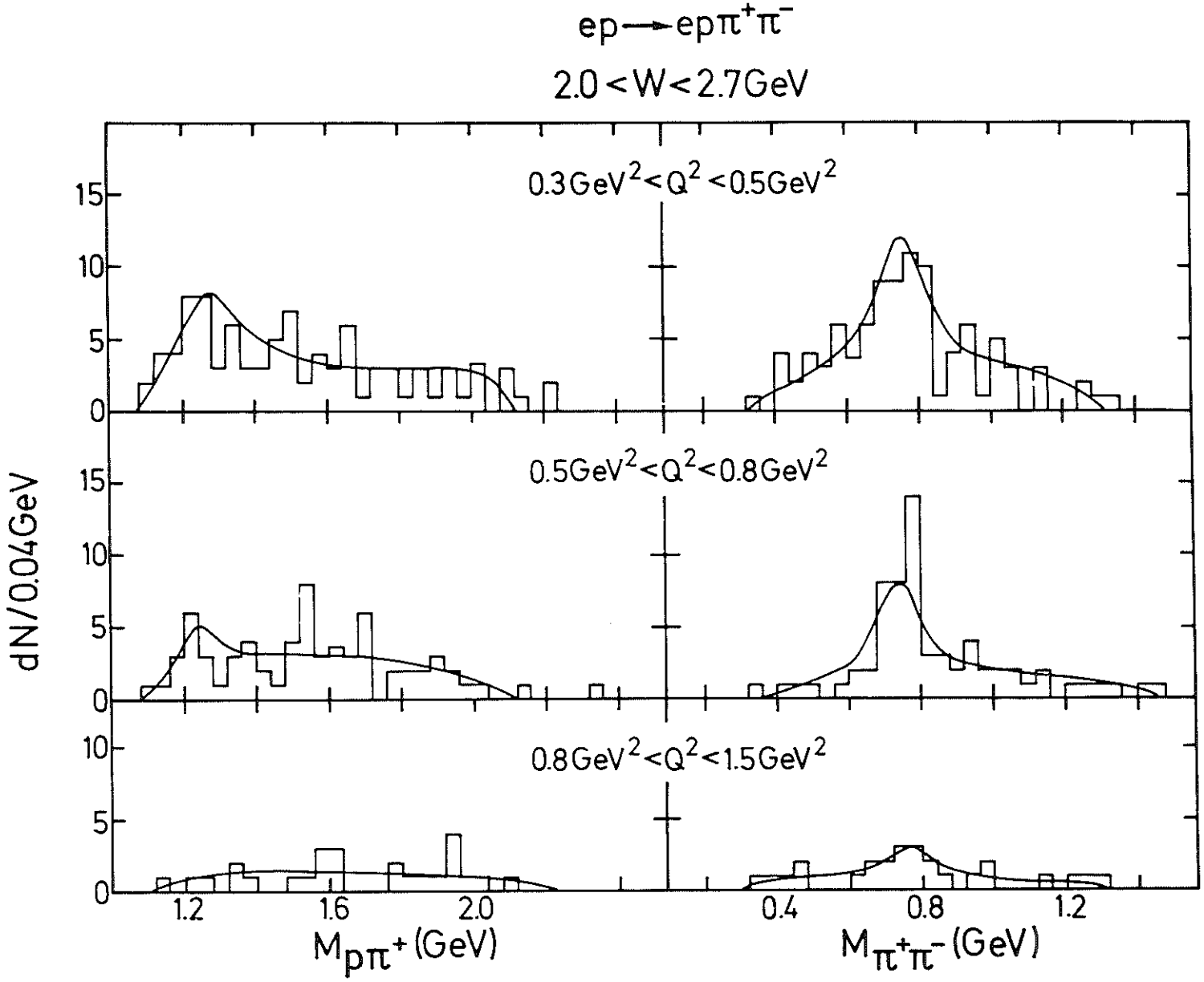
ep⟶epπ⁺π⁻
2.0<W<2.7GeV
0.3GeV²<Q²<0.5GeV²
0.5GeV²<Q²<0.8GeV²
0.8GeV²<Q²<1.5GeV²
dN/0.04GeV
15
10
5
0
1.2
1.6
2.0
0.4
0.8
1.2
Mpπ⁺ (GeV)
Mπ⁺π⁻ (GeV)

Fig. 12

SLAC

$\gamma_v P \longrightarrow \rho^0 P$

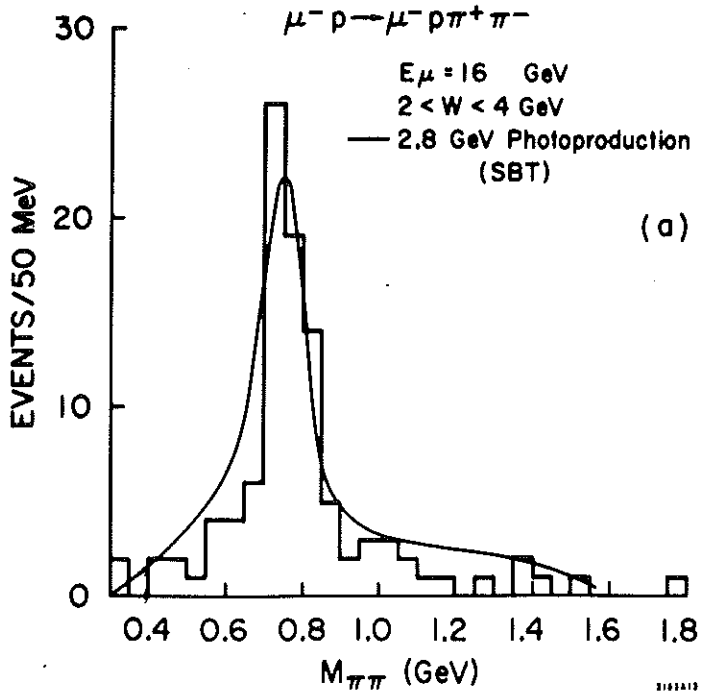

Fig. 13

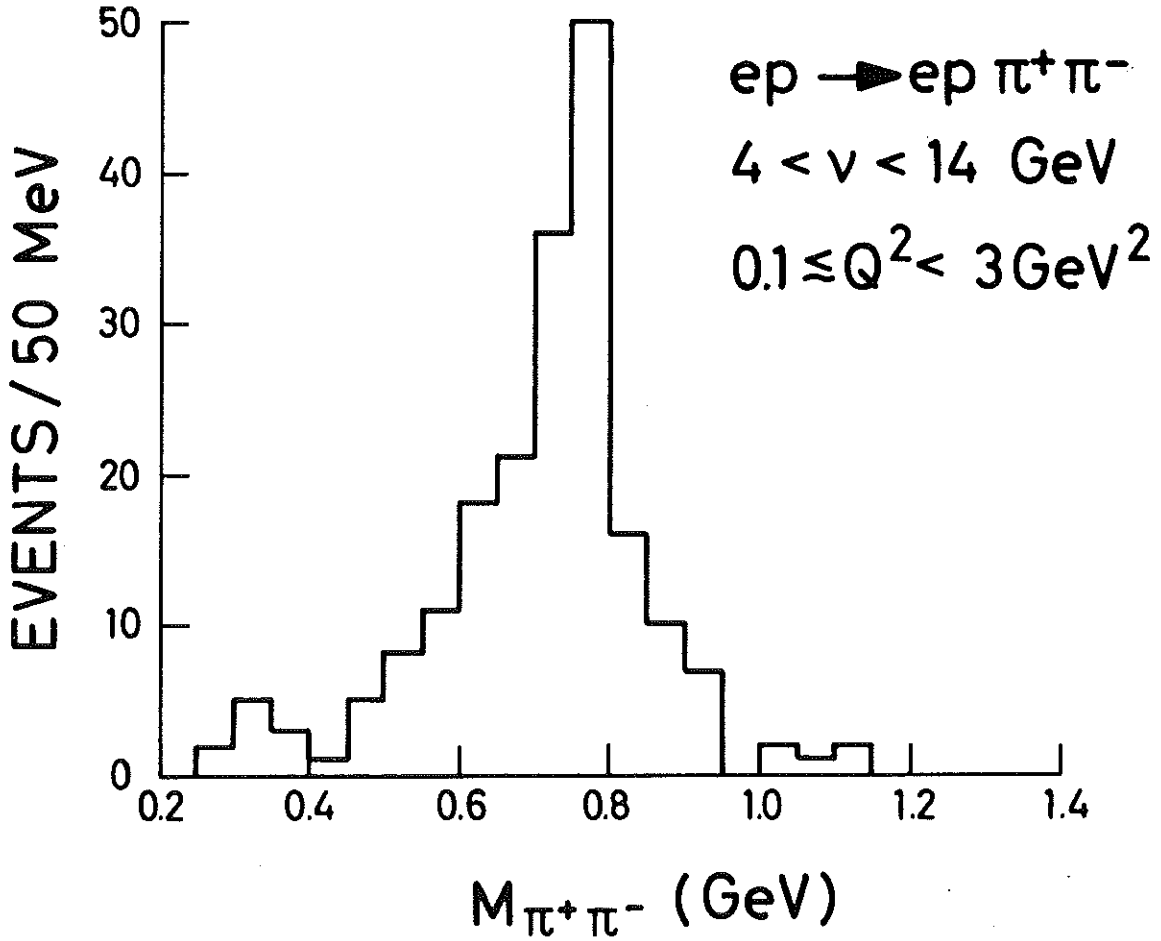

Fig. 14

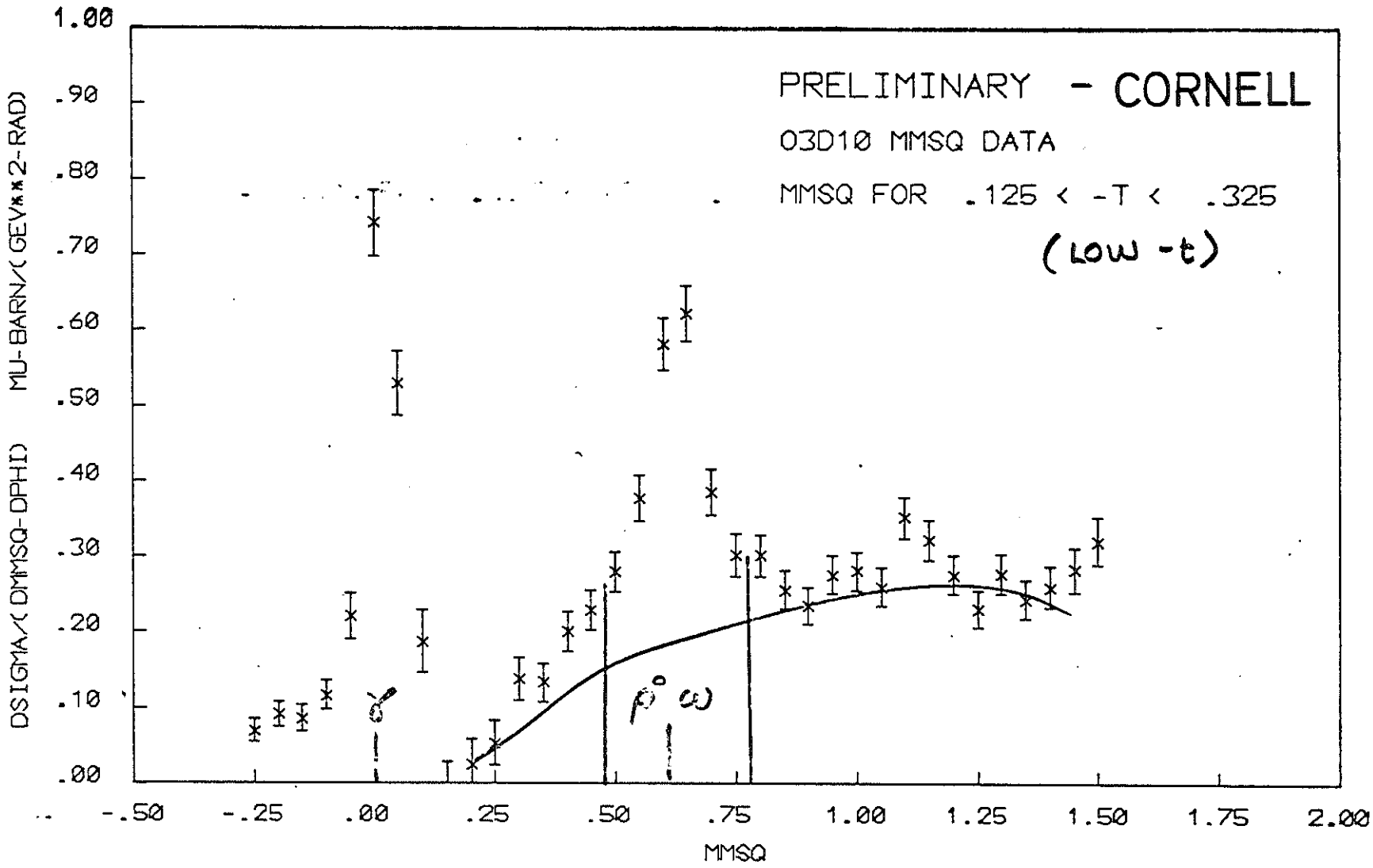
PRELIMINARY - CORNELL
03D10 MMSQ DATA
MMSQ FOR .125 < -T < .325
(low -t)
DSIGMA/(DMMSQ-DPHI) MU-BARN/(GEV** 2-RAD)
MMSQ
1.00
.90
.80
.70
.60
.50
.40
.30
.20
.10
.00
-.50
-.25
.00
.25
.50
.75
1.00
1.25
1.50
1.75
2.00
ρ° ω

Fig. 15

DESY

$ep \rightarrow ep\rho^0$

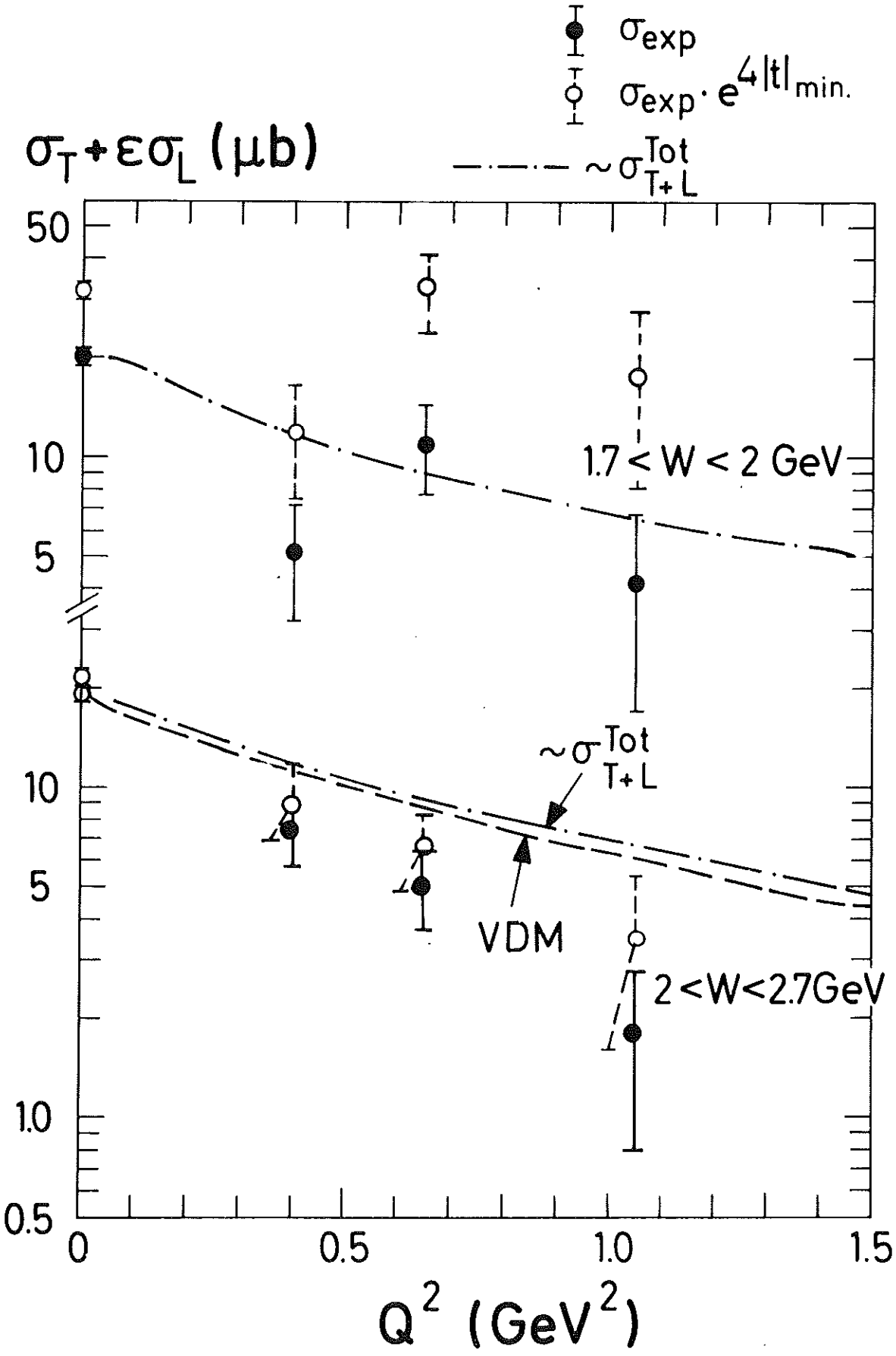

Fig. 16

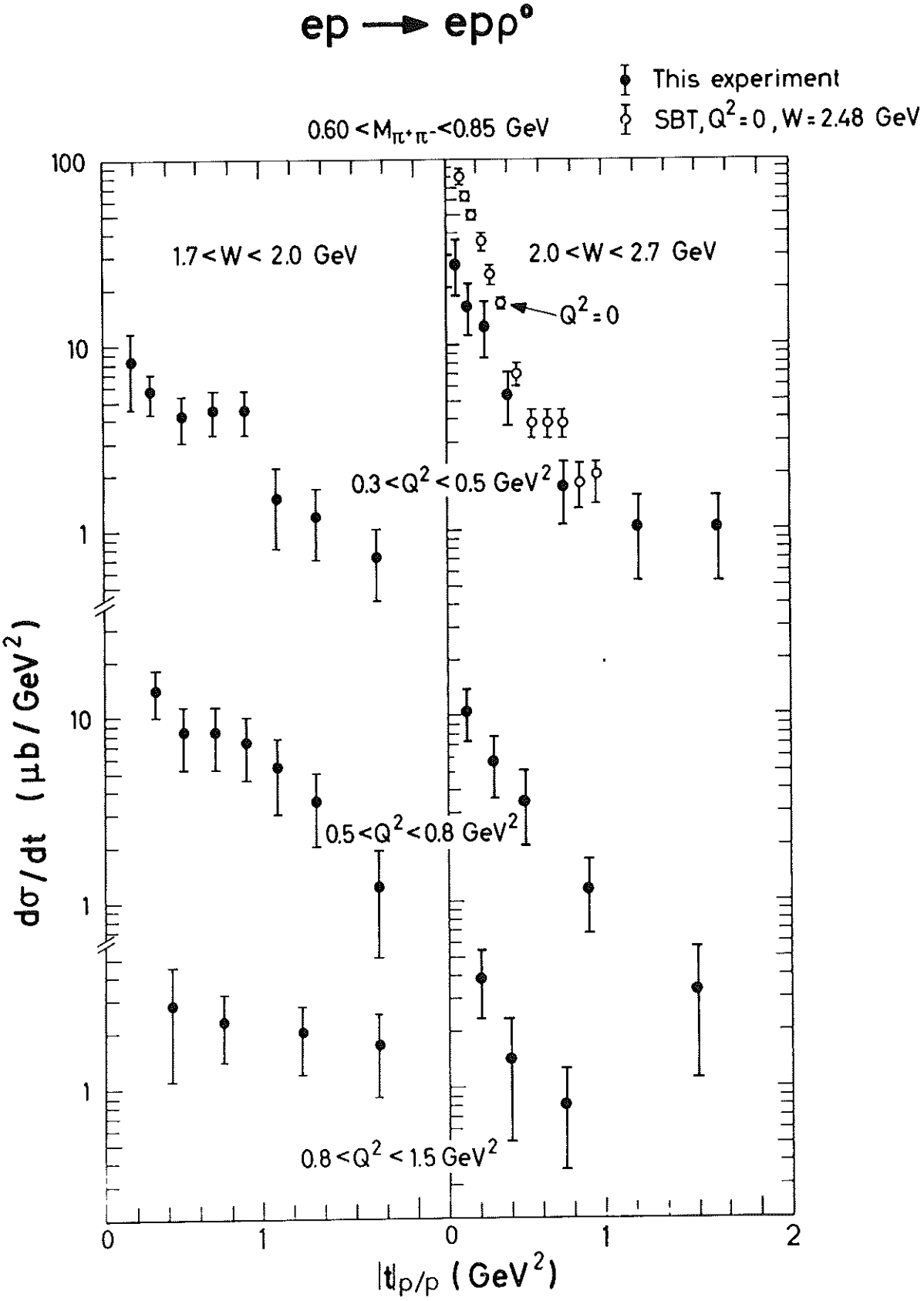
ep → epρ°
This experiment
SBT, Q² = 0, W = 2.48 GeV
0.60 < Mπ⁺π⁻ < 0.85 GeV
1.7 < W < 2.0 GeV
2.0 < W < 2.7 GeV
Q² = 0
0.3 < Q² < 0.5 GeV²
0.5 < Q² < 0.8 GeV²
0.8 < Q² < 1.5 GeV²
dσ/dt (μb/GeV²)
|t|p/p (GeV²)
100
10
1
0
1
2

Fig. 17

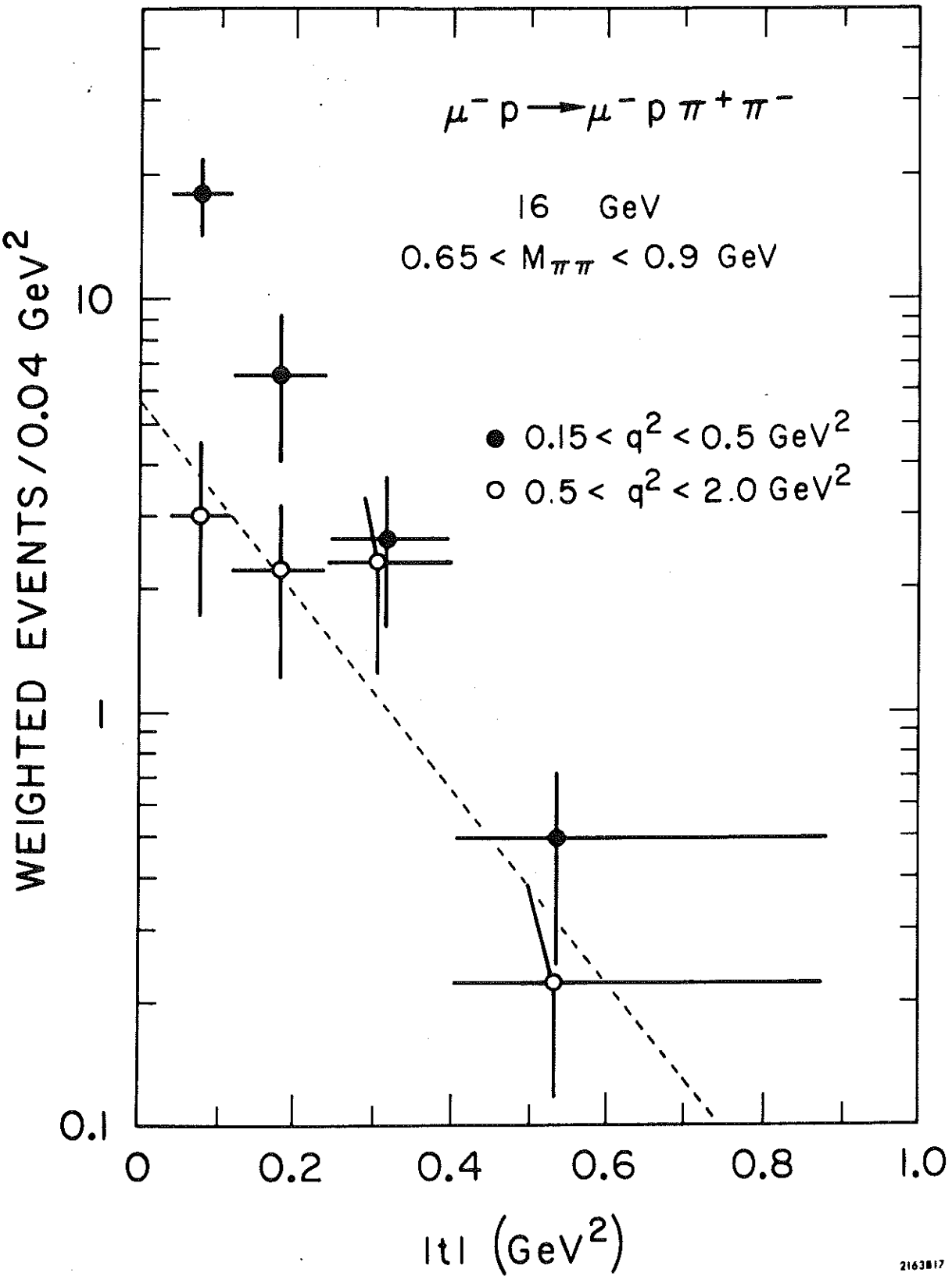
$\mu^- p \rightarrow \mu^- p \pi^+ \pi^-$
16 GeV
$0.65 < M_{\pi\pi} < 0.9$ GeV
● $0.15 < q^2 < 0.5$ GeV^2
○ $0.5 < q^2 < 2.0$ GeV^2
WEIGHTED EVENTS/0.04 GeV^2
10
1
0.1
0
0.2
0.4
0.6
0.8
1.0
$|t|$ (GeV^2)
2163B17

Fig. 18

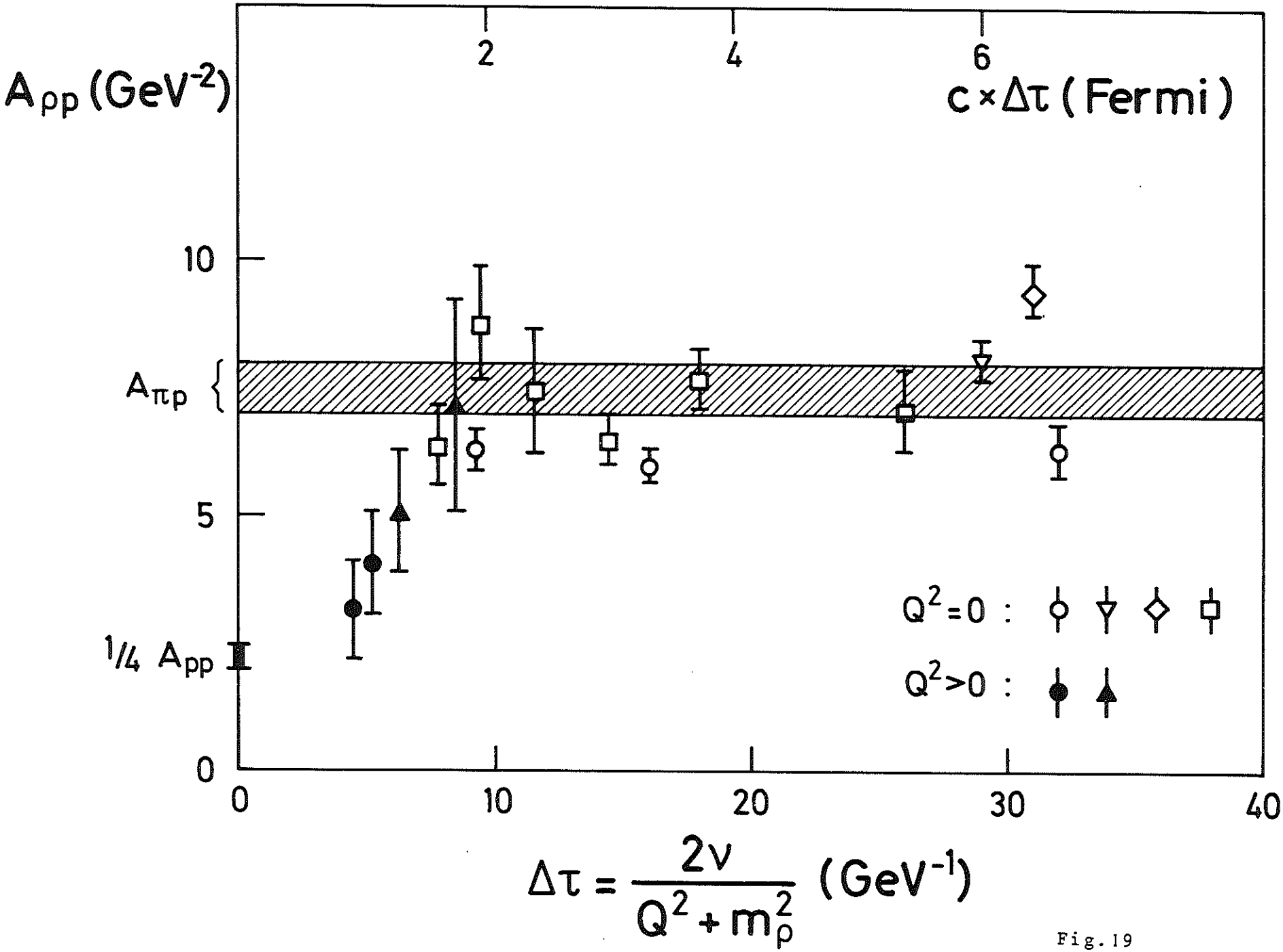
A_{pp} (GeV^{-2})
2
4
6
c × Δτ (Fermi)
10
$A_{\pi p}$
5
1/4 A_{pp}
0
0
10
20
30
40
Q^2=0 :
Q^2>0 :
$\Delta\tau = \frac{2\nu}{Q^2 + m_\rho^2}$ (GeV^{-1})

Fig. 19

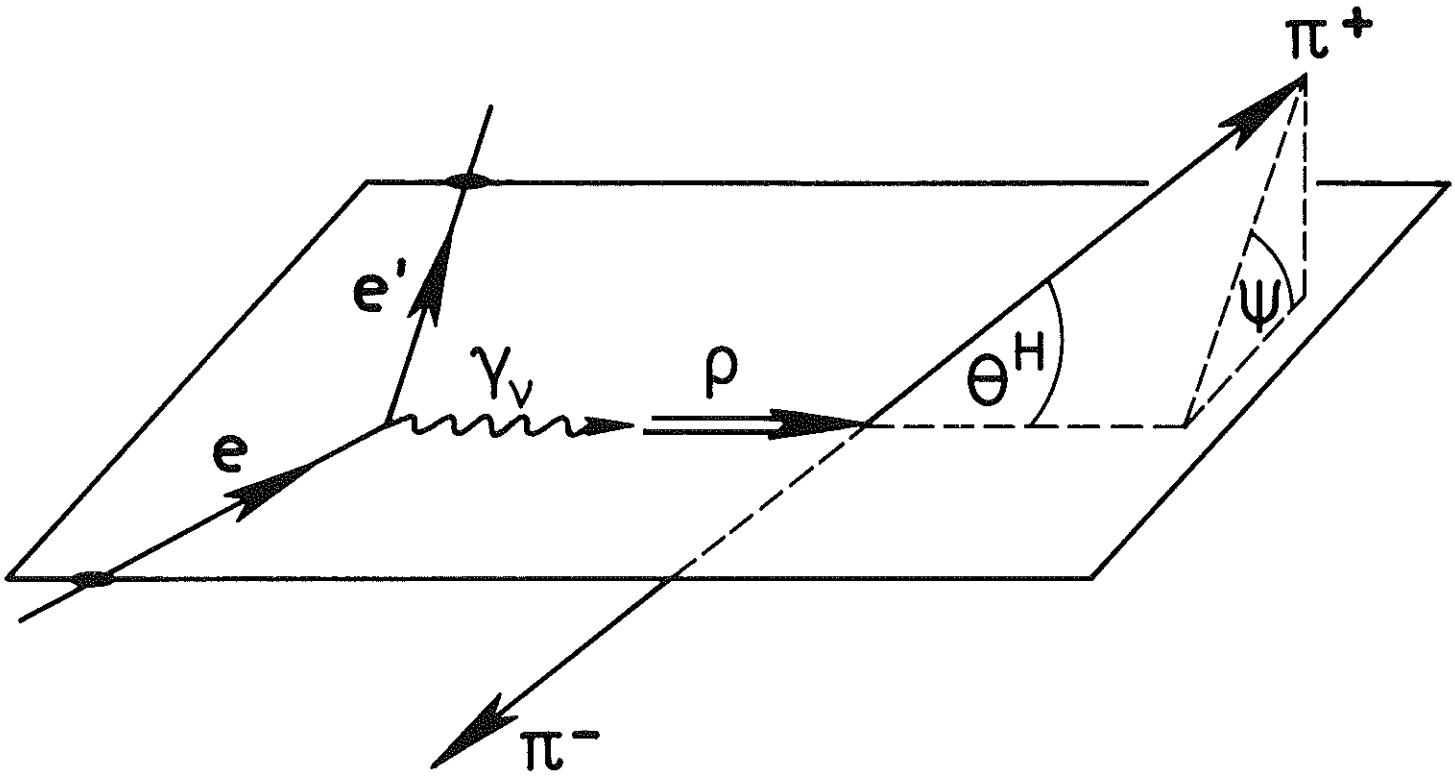

Fig. 20

SLAC - LBL - TUFTS

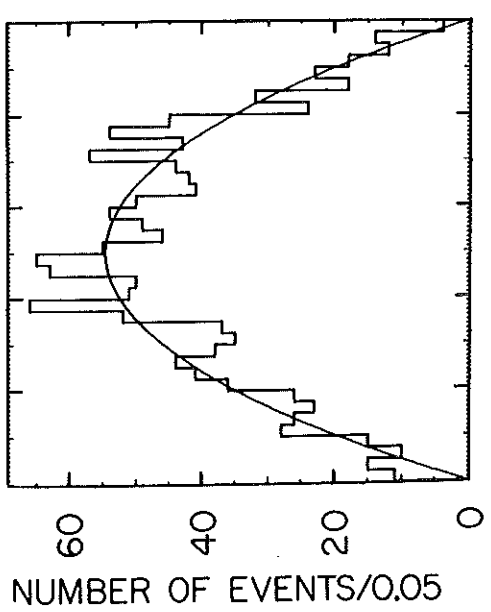

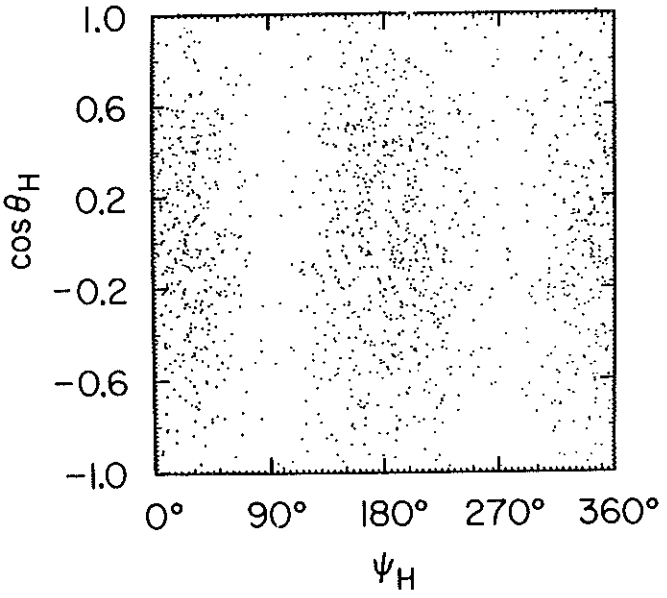

(b) $\gamma p \rightarrow p\pi^+\pi^-$

E_γ=4.7 GeV

$0.60 < M_{\pi\pi} < 0.85$ GeV

$0.02 < |t| < 0.4$ GeV^2

1457 EVENTS

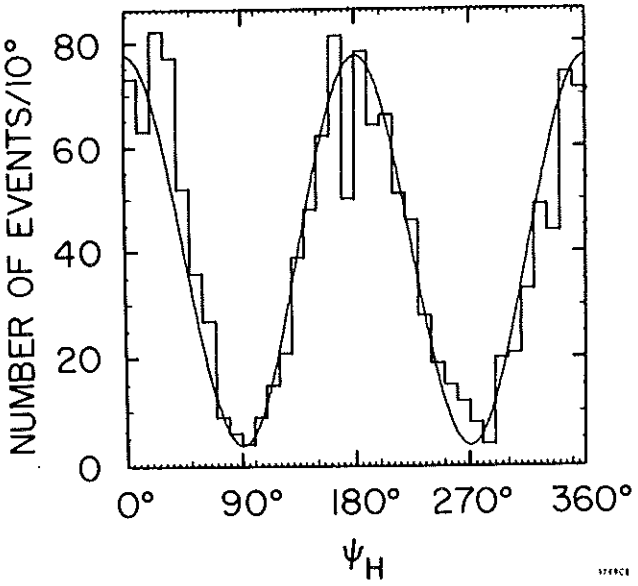

Fig. 21

DESY

$ep \rightarrow ep\rho^0$

$0.65 < M_{\pi^+\pi^-} < 0.84\,GeV \qquad 0.3 < Q^2 < 1.5\,GeV^2$

$2.0 < W < 2.7\,GeV$

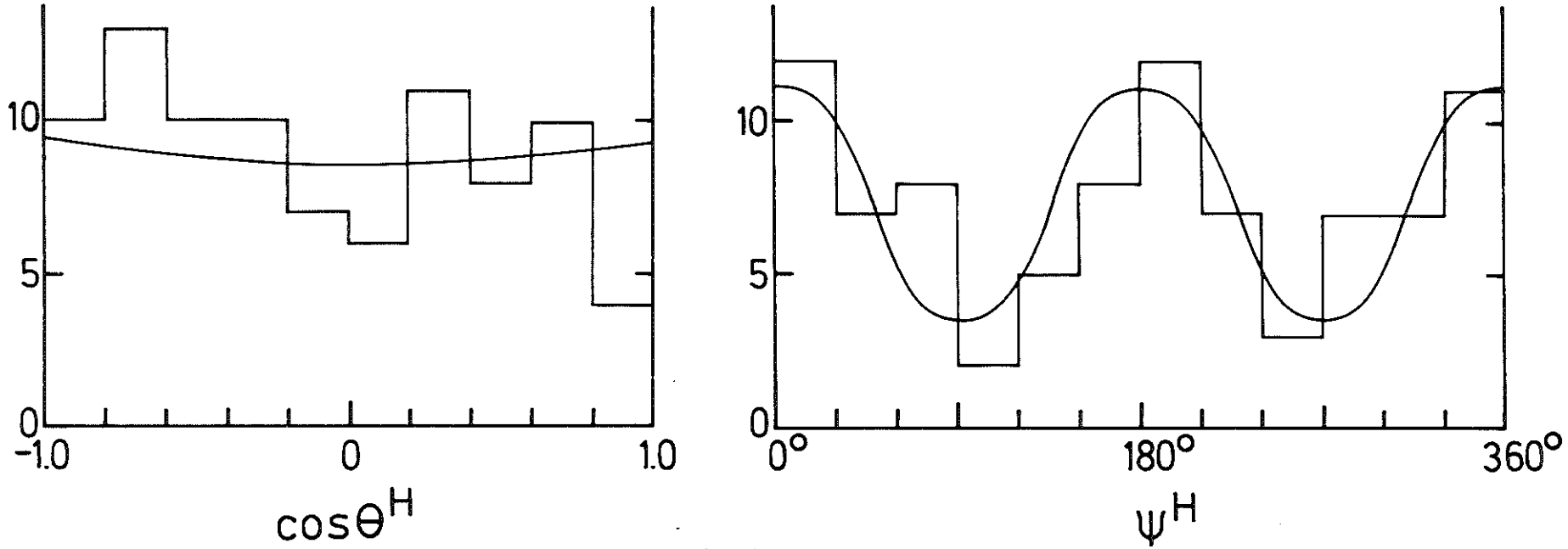

Fig.22

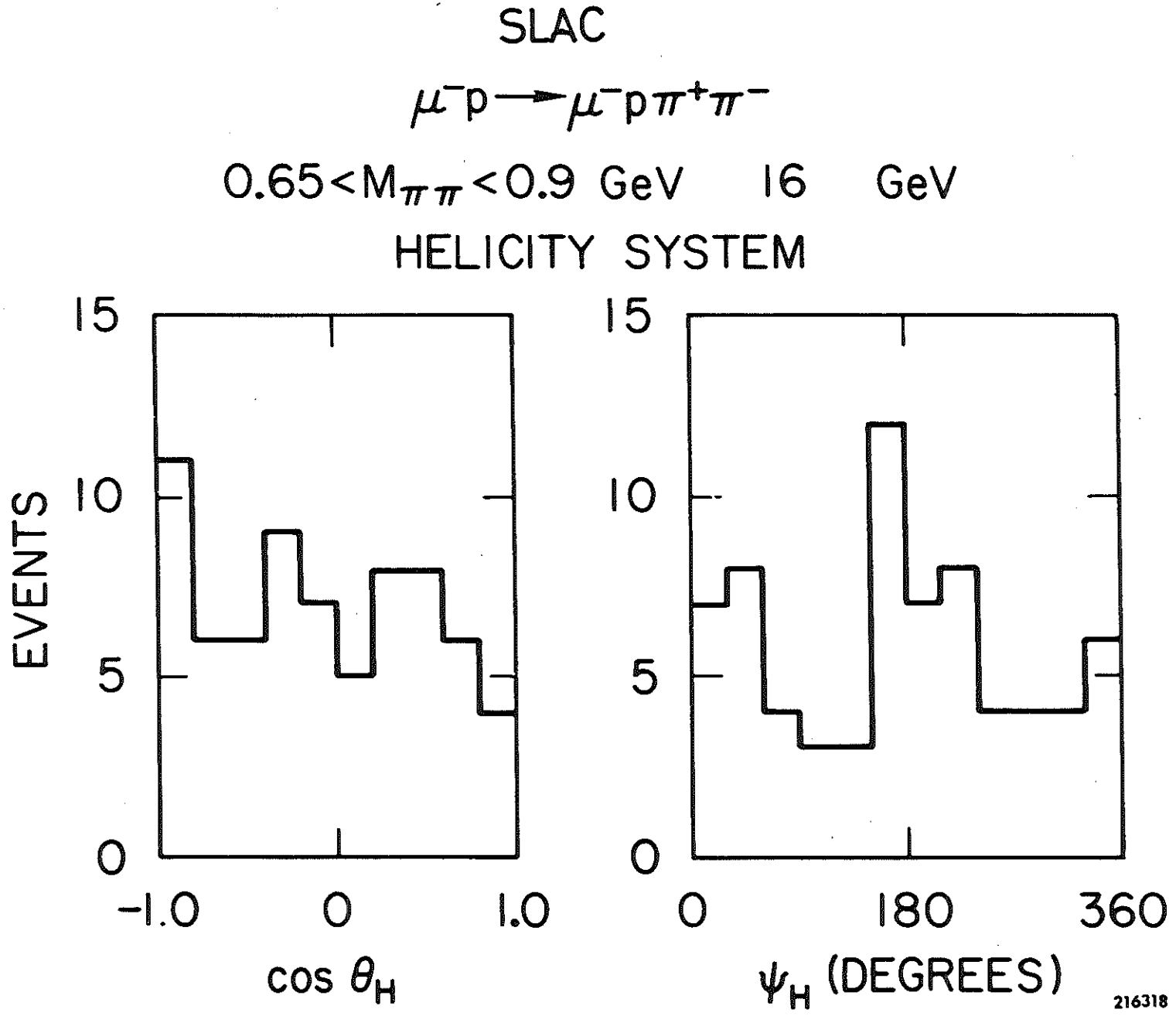
SLAC
$\mu^- p \rightarrow \mu^- p \pi^+ \pi^-$
$0.65 < M_{\pi\pi} < 0.9$ GeV 16 GeV
HELICITY SYSTEM
EVENTS
15
10
5
0
-1.0
0
1.0
$\cos \theta_H$
15
10
5
0
0
180
360
ψ_H (DEGREES)
216318

Fig.23

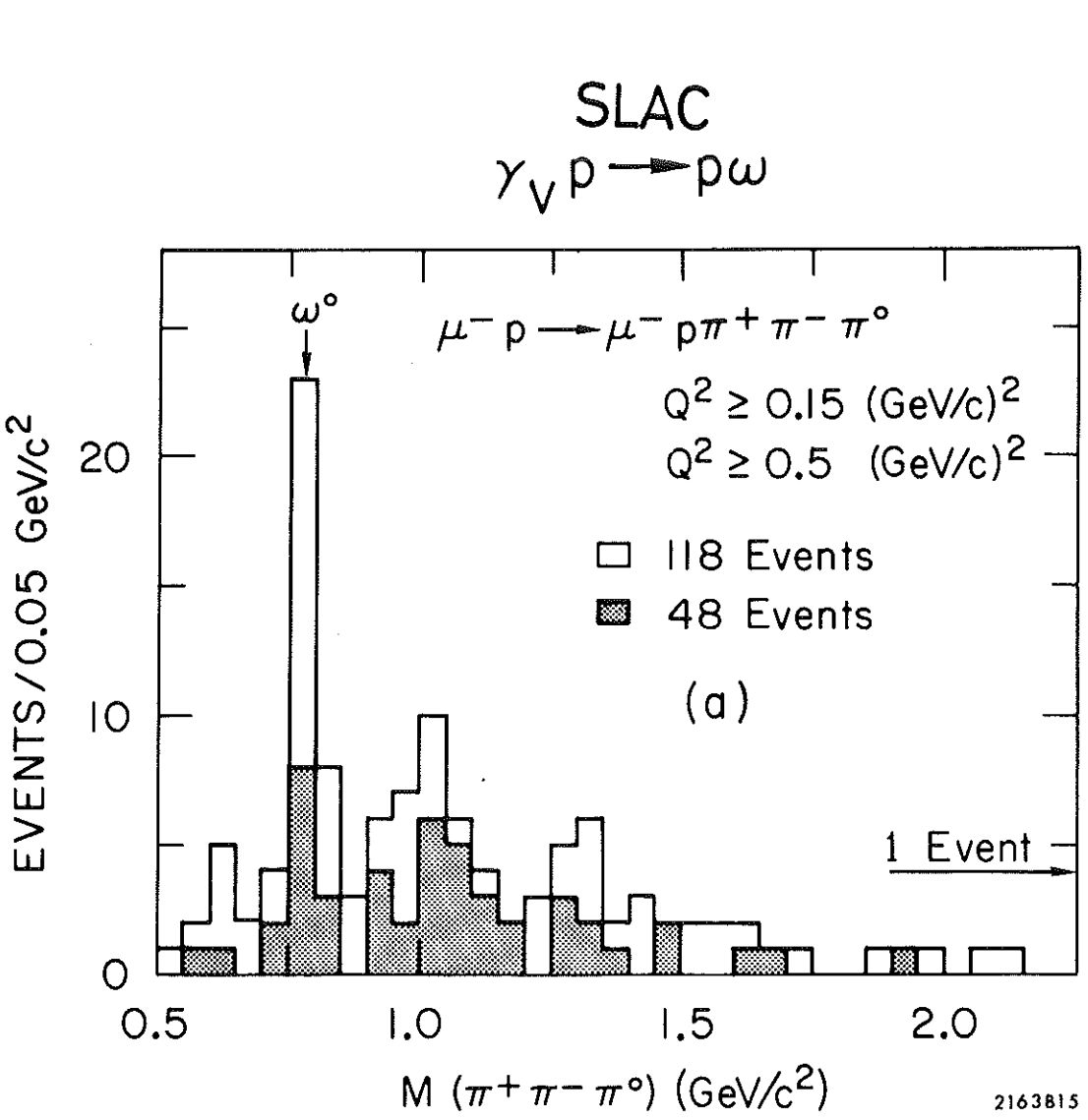
SLAC
$\gamma_V p \rightarrow p\omega$
ω°
$\mu^- p \rightarrow \mu^- p\pi^+\pi^-\pi^\circ$
$Q^2 \geq 0.15$ (GeV/c)^2
$Q^2 \geq 0.5$ (GeV/c)^2
118 Events
48 Events
(a)
1 Event
EVENTS/0.05 GeV/c^2
M ($\pi^+\pi^-\pi^\circ$) (GeV/c^2)
2163815

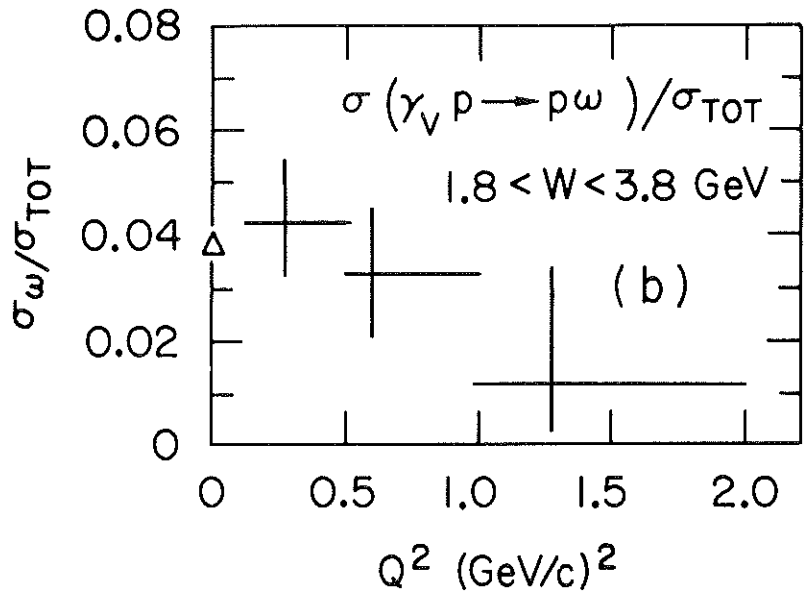
$\sigma(\gamma_V p \rightarrow p\omega)/\sigma_{TOT}$
1.8 < W < 3.8 GeV
(b)
$\sigma_\omega/\sigma_{TOT}$
Q^2 (GeV/c)^2

Fig. 24

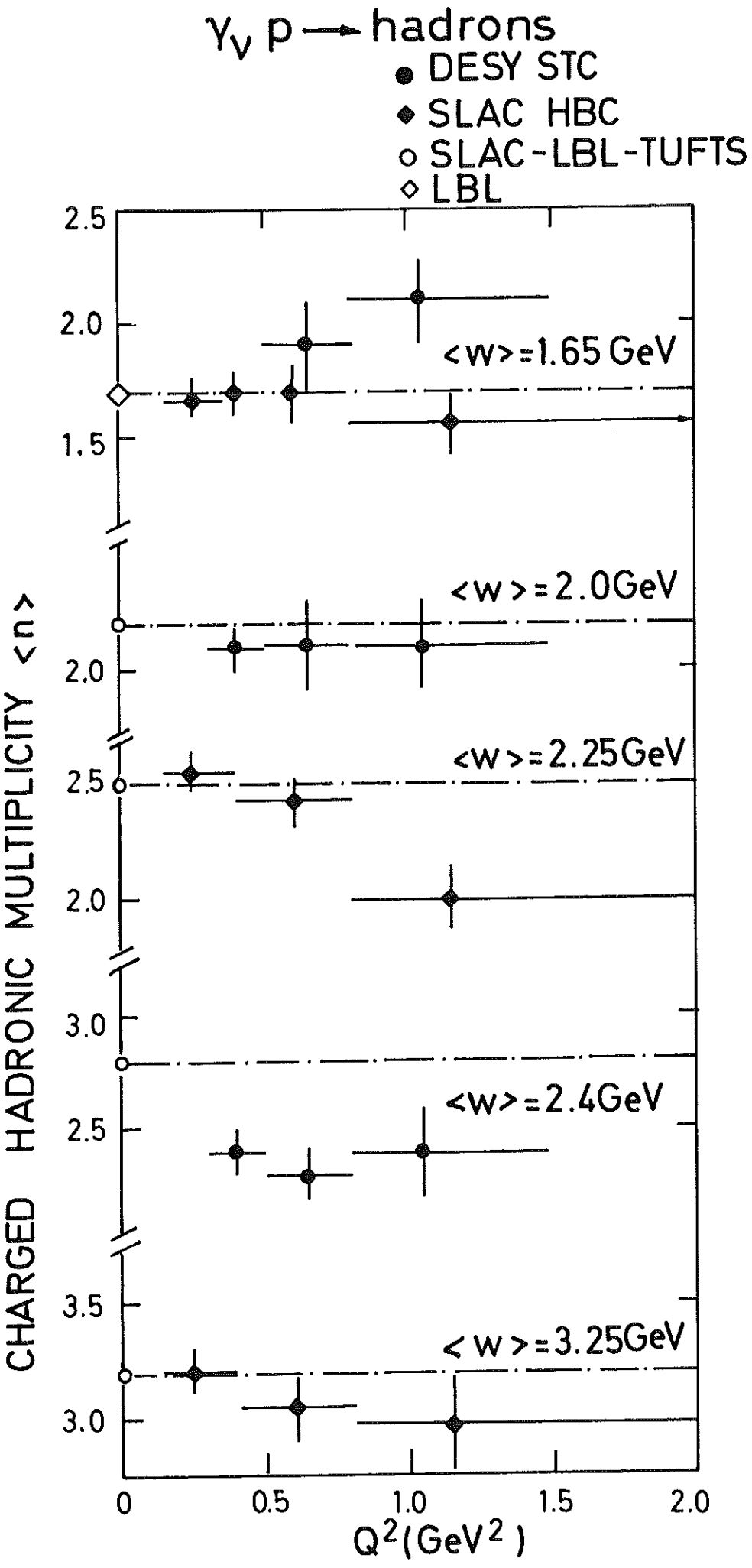
$\gamma_V p \rightarrow$ hadrons
DESY STC
SLAC HBC
SLAC-LBL-TUFTS
LBL
<W>=1.65 GeV
<W>=2.0GeV
<W>=2.25GeV
<W>=2.4GeV
<W>=3.25GeV
CHARGED HADRONIC MULTIPLICITY <n>
Q^2(GeV^2)
2.5
2.0
1.5
2.0
2.5
2.0
3.0
2.5
3.5
3.0
0
0.5
1.0
1.5
2.0

Fig.25

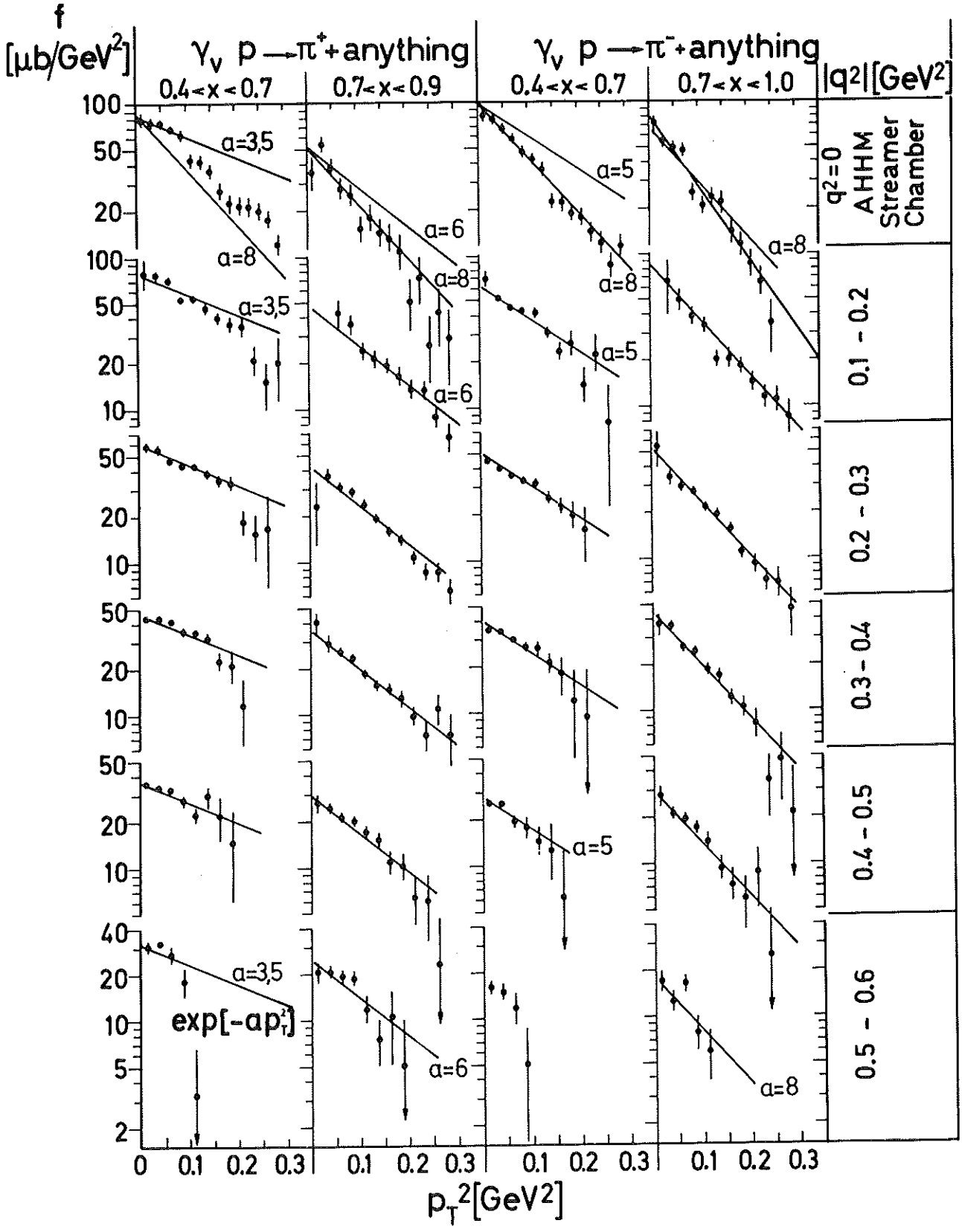
f
[μb/GeV²]
γv p → π⁺ + anything
γv p → π⁻ + anything
0.4 < x < 0.7
0.7 < x < 0.9
0.4 < x < 0.7
0.7 < x < 1.0
|q²| [GeV²]
q²=0 AHHM Streamer Chamber
0.1 - 0.2
0.2 - 0.3
0.3 - 0.4
0.4 - 0.5
0.5 - 0.6
a=3,5
a=6
a=8
a=5
exp[-ap_T²]
p_T² [GeV²]

Fig.26

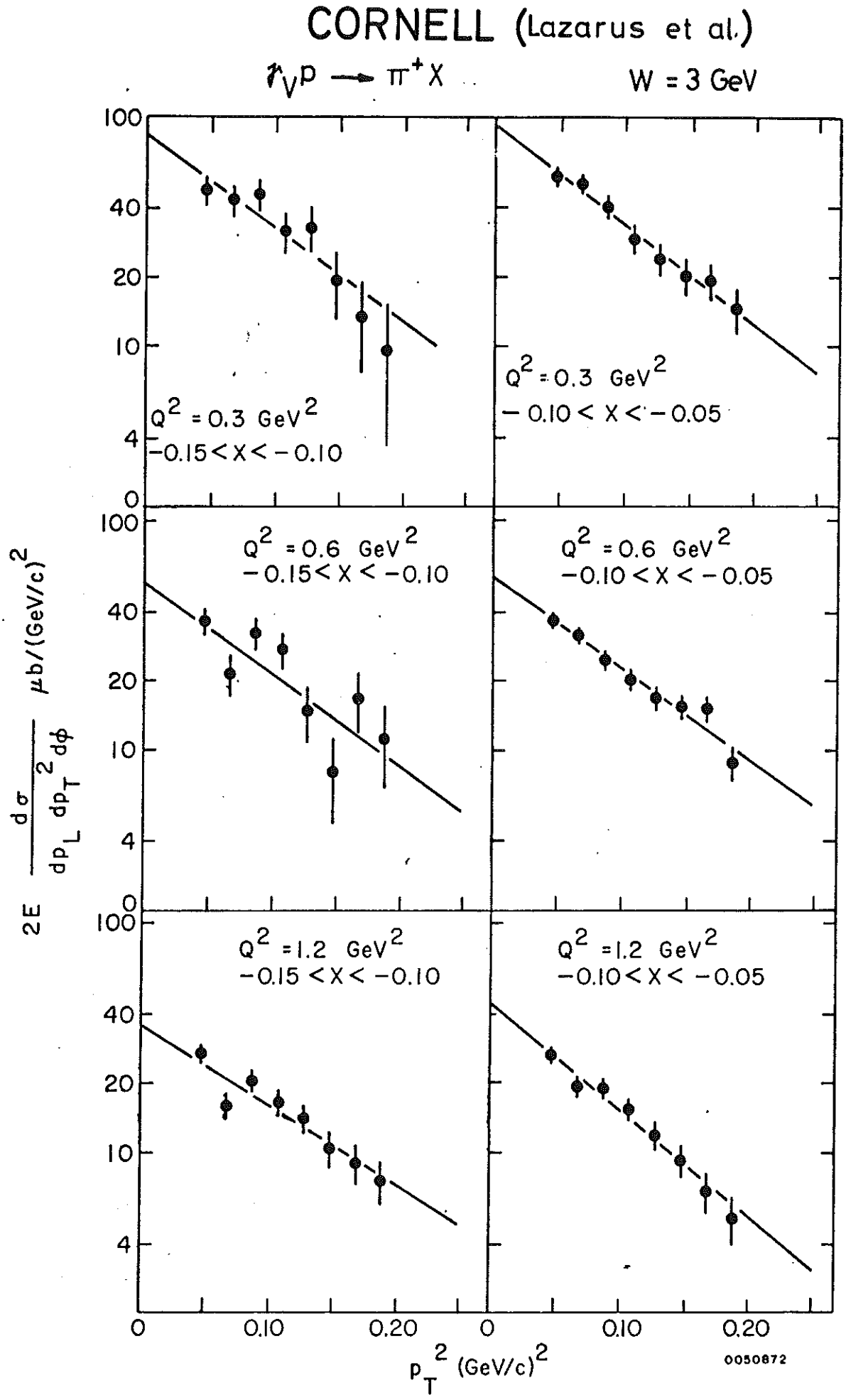
CORNELL (Lazarus et al.)
$\nu_V p \rightarrow \pi^+ X$
W = 3 GeV
Q^2 = 0.3 GeV^2
−0.15 < X < −0.10
Q^2 = 0.3 GeV^2
− 0.10 < X < − 0.05
Q^2 = 0.6 GeV^2
−0.15 < X < −0.10
Q^2 = 0.6 GeV^2
−0.10 < X < −0.05
Q^2 = 1.2 GeV^2
−0.15 < X < −0.10
Q^2 = 1.2 GeV^2
−0.10 < X < −0.05
$2E \frac{d\sigma}{dp_L dp_T^2 d\phi}$ μb/(GeV/c)^2
p_T^2 (GeV/c)^2
0050872

Fig.27

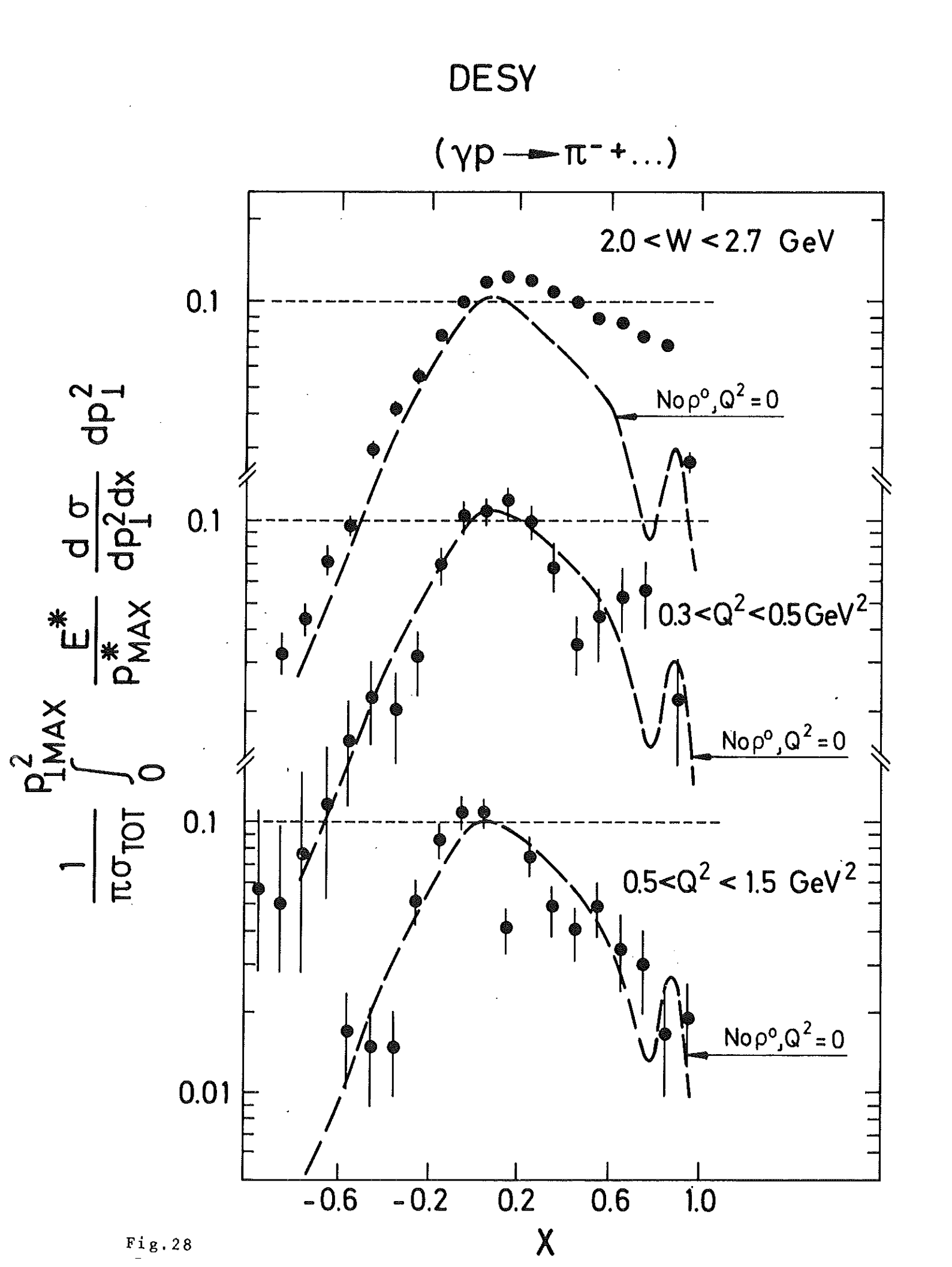
DESY
(γp → π⁻ + ...)
2.0 < W < 2.7 GeV
No ρ°, Q² = 0
0.3 < Q² < 0.5 GeV²
No ρ°, Q² = 0
0.5 < Q² < 1.5 GeV²
No ρ°, Q² = 0
0.1
0.1
0.1
0.01
-0.6
-0.2
0.2
0.6
1.0
X
$\frac{1}{\pi\sigma_{TOT}} \int_0^{P_{T\,MAX}^2} \frac{E^*}{P^*_{MAX}} \frac{d\sigma}{dp_T^2 dx} dp_T^2$

Fig. 28

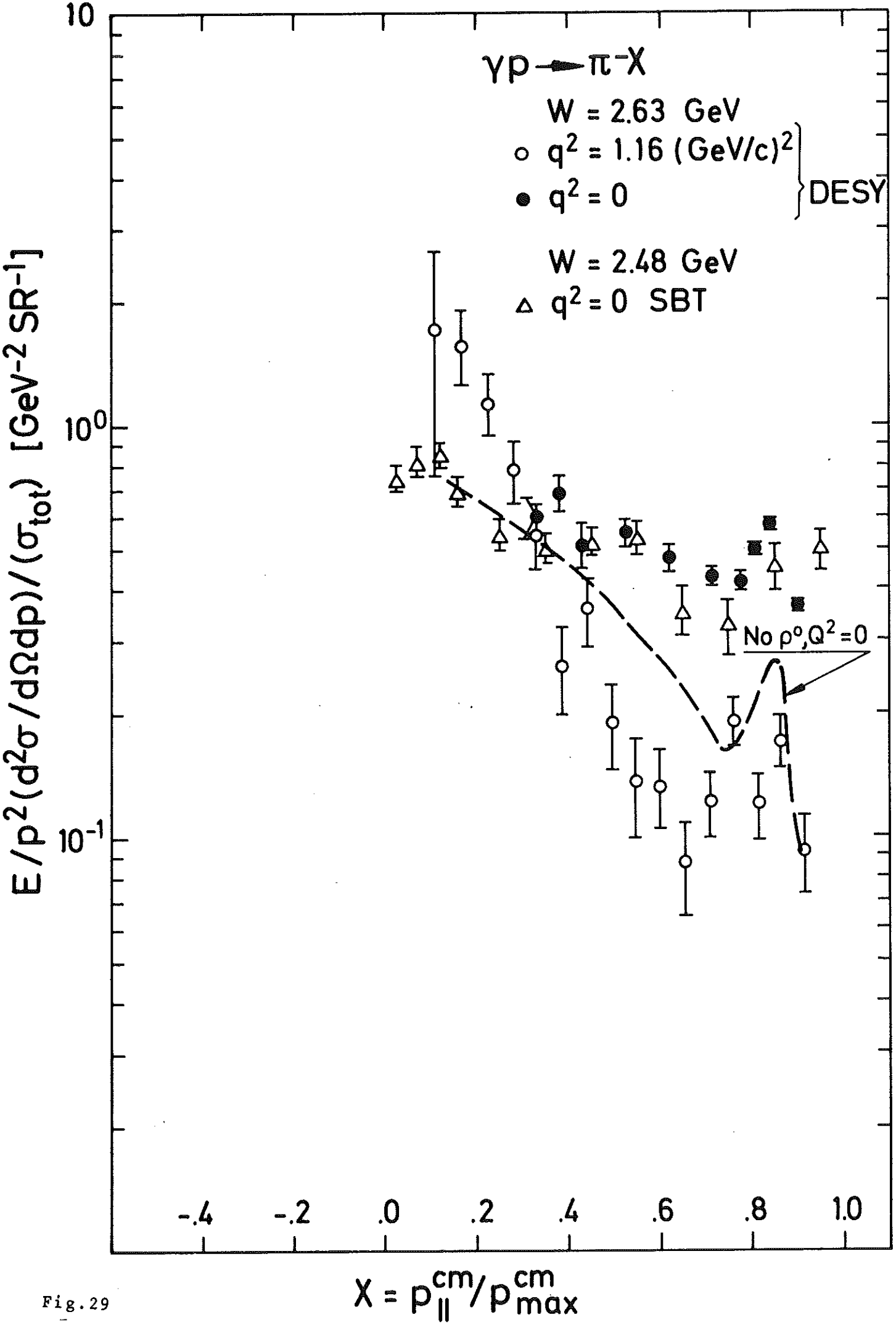
γp → π⁻X
W = 2.63 GeV
q² = 1.16 (GeV/c)²
q² = 0
DESY
W = 2.48 GeV
q² = 0 SBT
No ρ°, Q² = 0
E/p²(d²σ/dΩdp)/(σtot) [GeV⁻² SR⁻¹]
10
10⁰
10⁻¹
-.4
-.2
.0
.2
.4
.6
.8
1.0
X = p∥cm/pmaxcm

Fig. 29

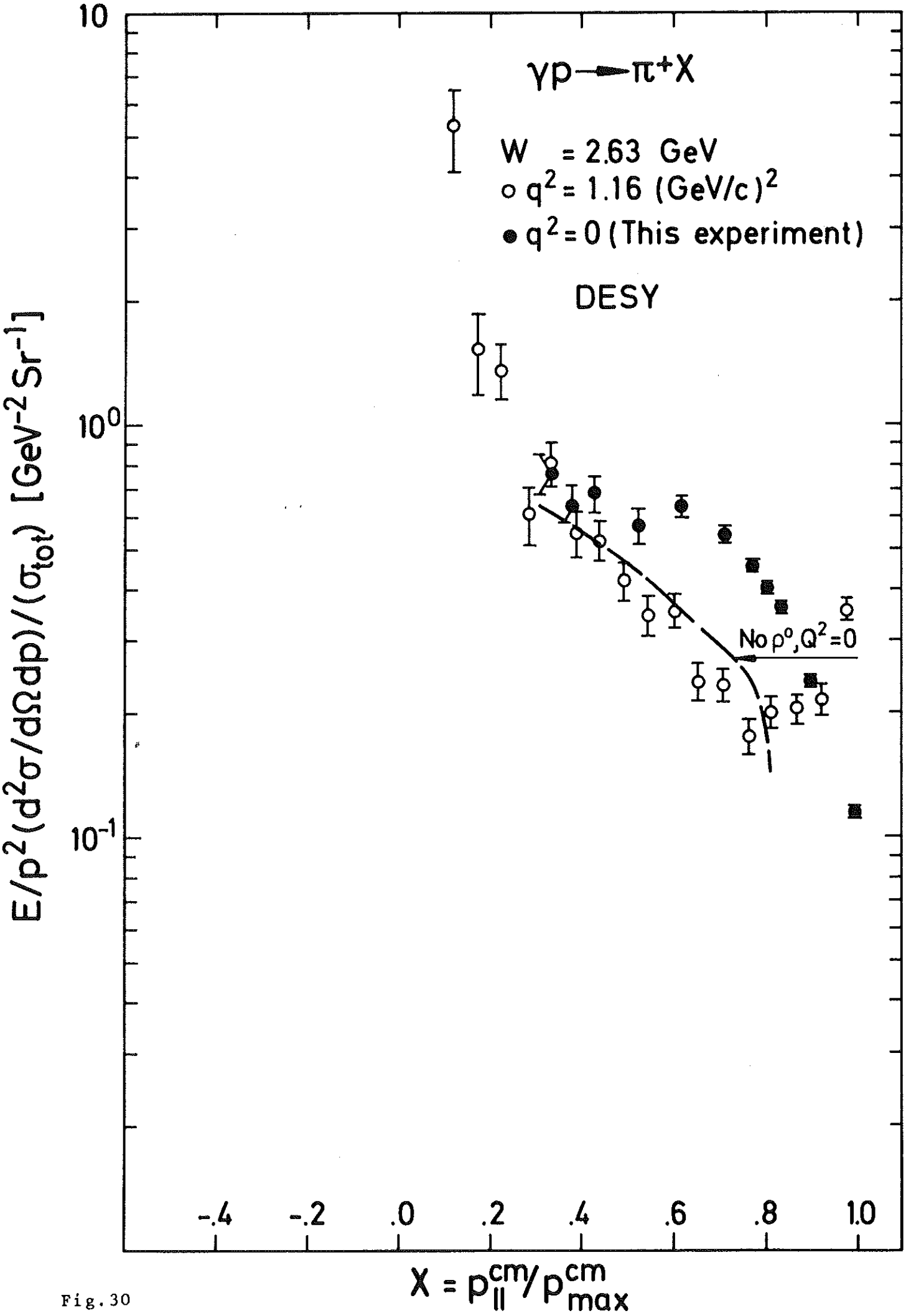
10
10^0
10^{-1}
$\gamma p \rightarrow \pi^+ X$
W = 2.63 GeV
○ q^2 = 1.16 (GeV/c)^2
● q^2 = 0 (This experiment)
DESY
No ρ^0, Q^2=0
$E/p^2(d^2\sigma/d\Omega dp)/(\sigma_{tot})$ [GeV^{-2}Sr^{-1}]
-.4
-.2
.0
.2
.4
.6
.8
1.0
$X = p_{||}^{cm}/p_{max}^{cm}$

Fig. 30

DESY

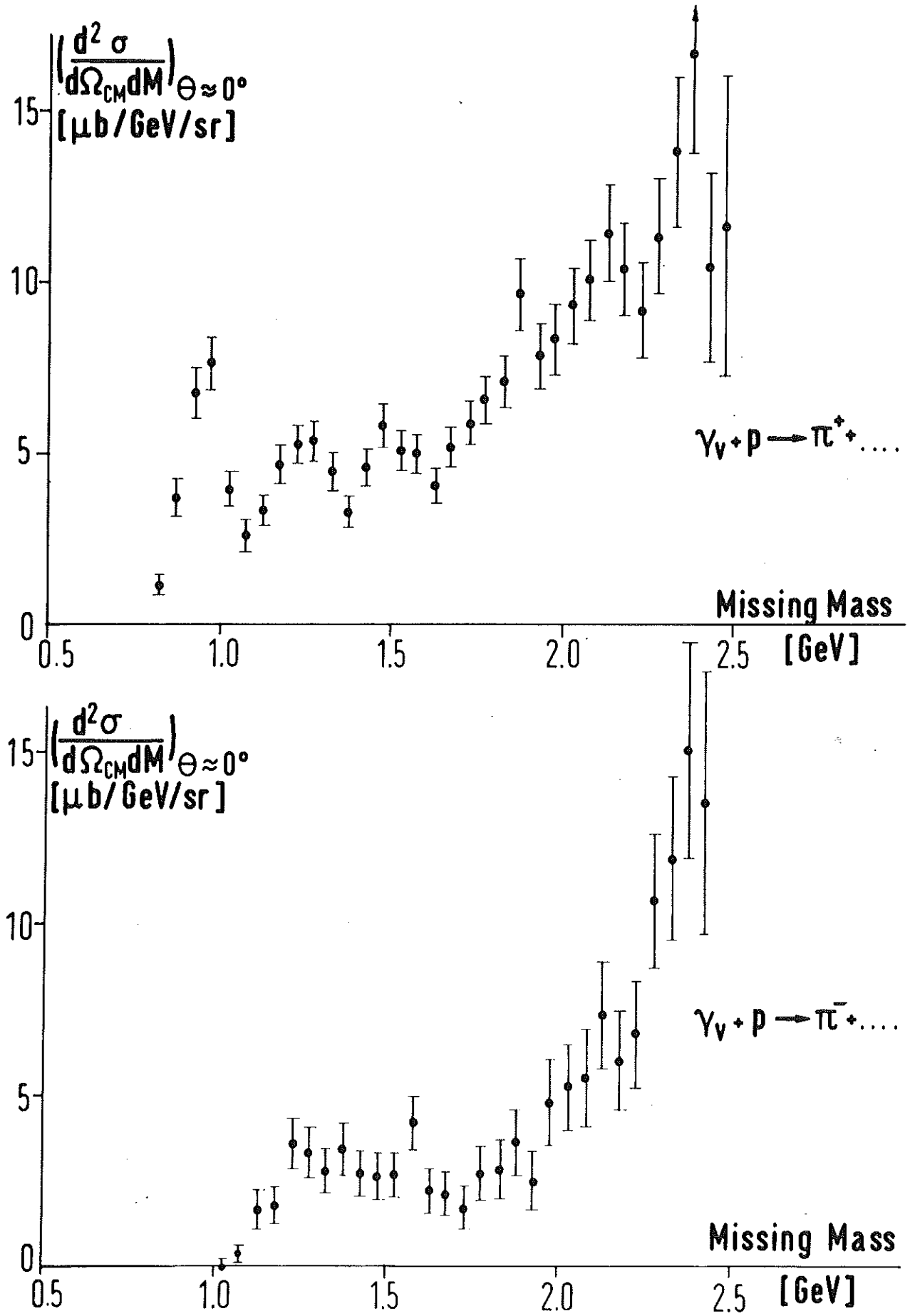
$\left(\frac{d^2\sigma}{d\Omega_{CM}dM}\right)_{\Theta\approx 0°}$
[μb/GeV/sr]
15
10
5
0
$\gamma_V + p \rightarrow \pi^+ + \ldots$
Missing Mass
0.5
1.0
1.5
2.0
2.5
[GeV]
$\left(\frac{d^2\sigma}{d\Omega_{CM}dM}\right)_{\Theta\approx 0°}$
[μb/GeV/sr]
15
10
5
0
$\gamma_V + p \rightarrow \pi^- + \ldots$
Missing Mass
0.5
1.0
1.5
2.0
2.5
[GeV]

Fig. 31

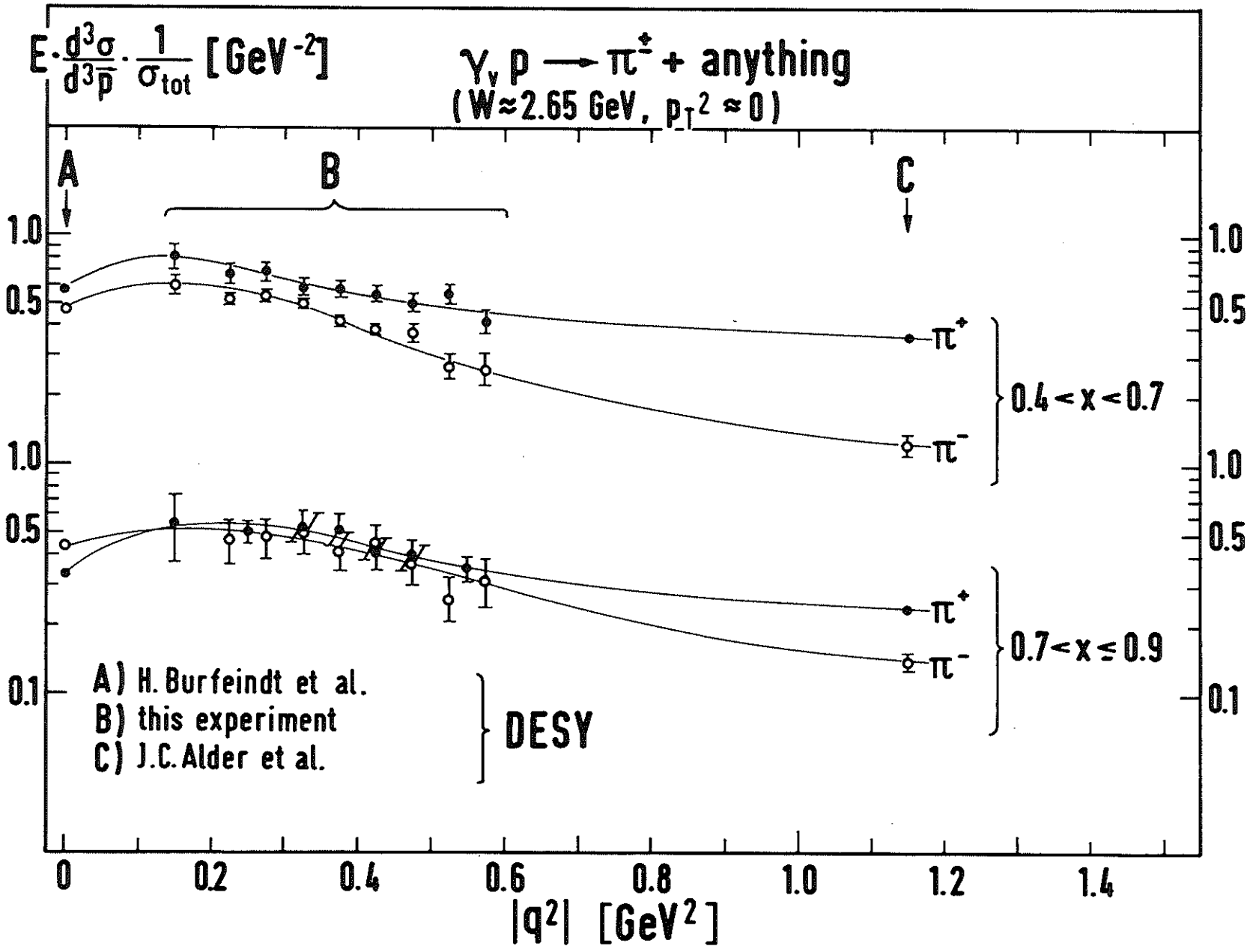
E·d³σ/d³p·1/σtot [GeV⁻²]
γv p → π± + anything
(W≈2.65 GeV, pT² ≈ 0)
A
B
C
1.0
0.5
1.0
0.5
0.1
π+
π−
0.4<x<0.7
0.7<x≤0.9
A) H. Burfeindt et al.
B) this experiment
C) J.C. Alder et al.
DESY
0
0.2
0.4
0.6
0.8
1.0
1.2
1.4
|q²| [GeV²]

Fig. 32

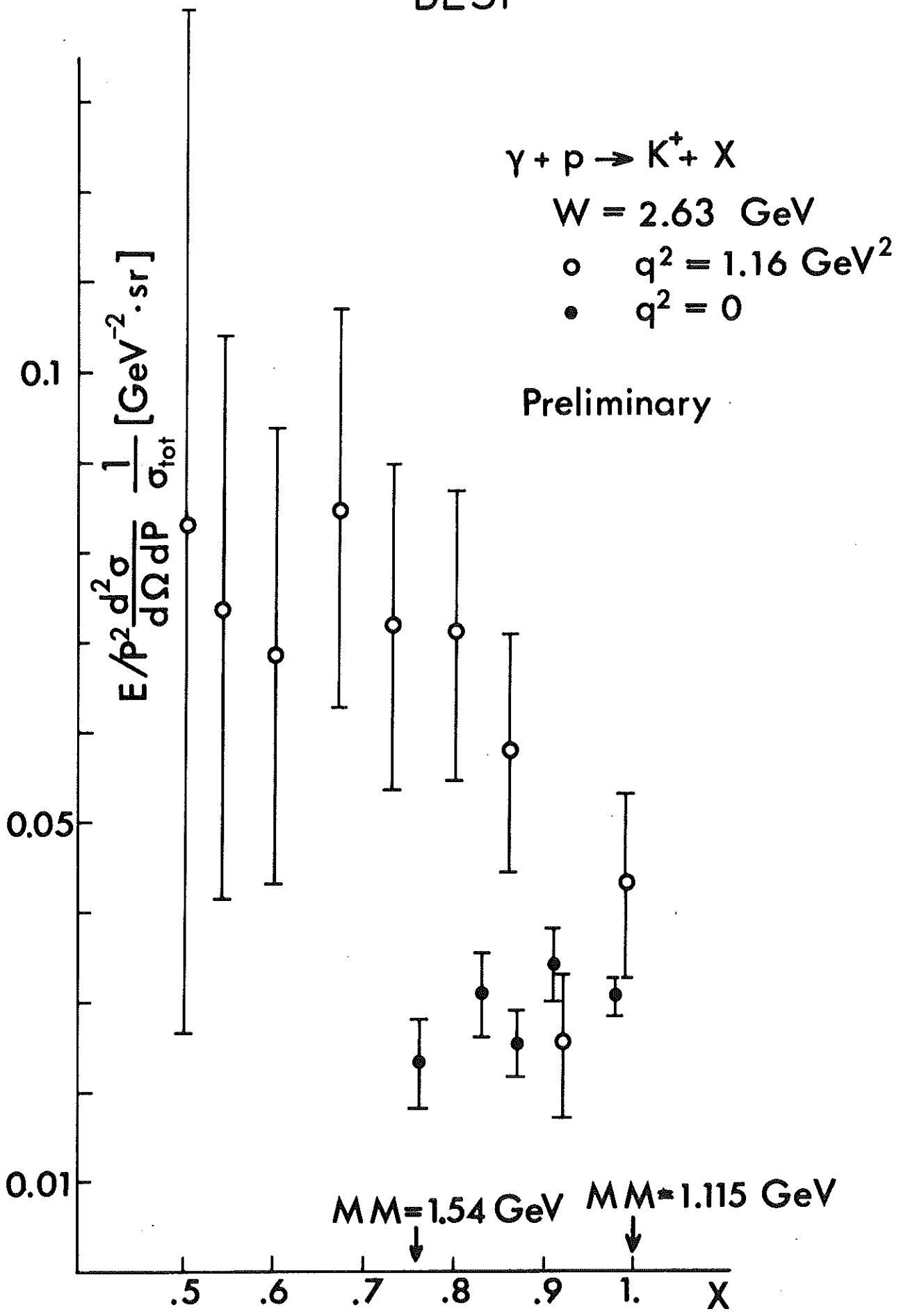
DESY
γ + p → K⁺ + X
W = 2.63 GeV
q² = 1.16 GeV²
q² = 0
Preliminary
E/p² d²σ/dΩdP 1/σtot [GeV⁻².sr]
0.1
0.05
0.01
MM=1.54 GeV
MM=1.115 GeV
.5
.6
.7
.8
.9
1.
X

Fig.33

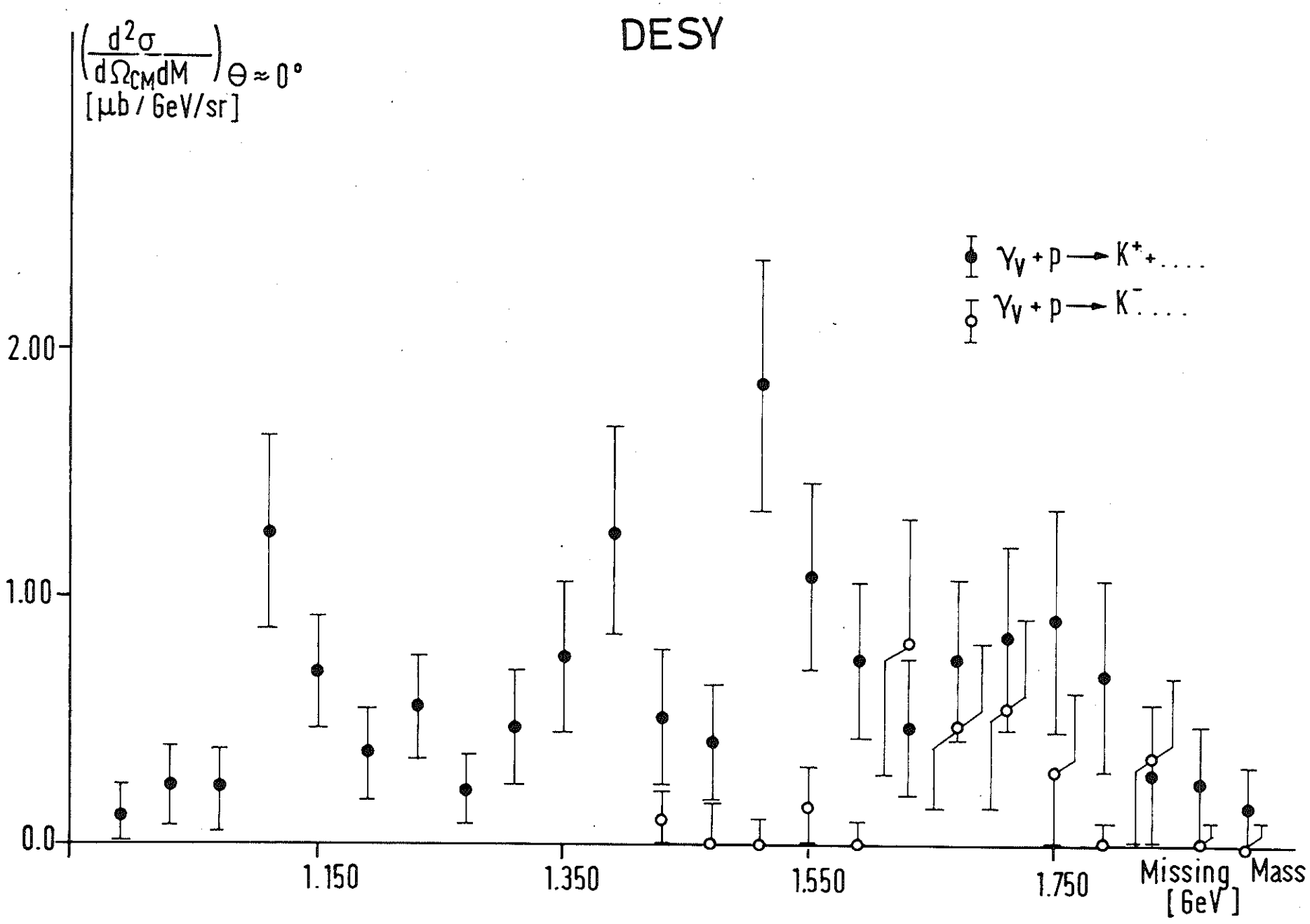
DESY
$\left(\frac{d^2\sigma}{d\Omega_{CM}dM}\right)_{\Theta \approx 0°}$
[μb / GeV/sr]
$\gamma_V + p \rightarrow K^+ + \ldots$
$\gamma_V + p \rightarrow K^- \ldots$
2.00
1.00
0.0
1.150
1.350
1.550
1.750
Missing Mass
[GeV]

Fig. 34

SLAC

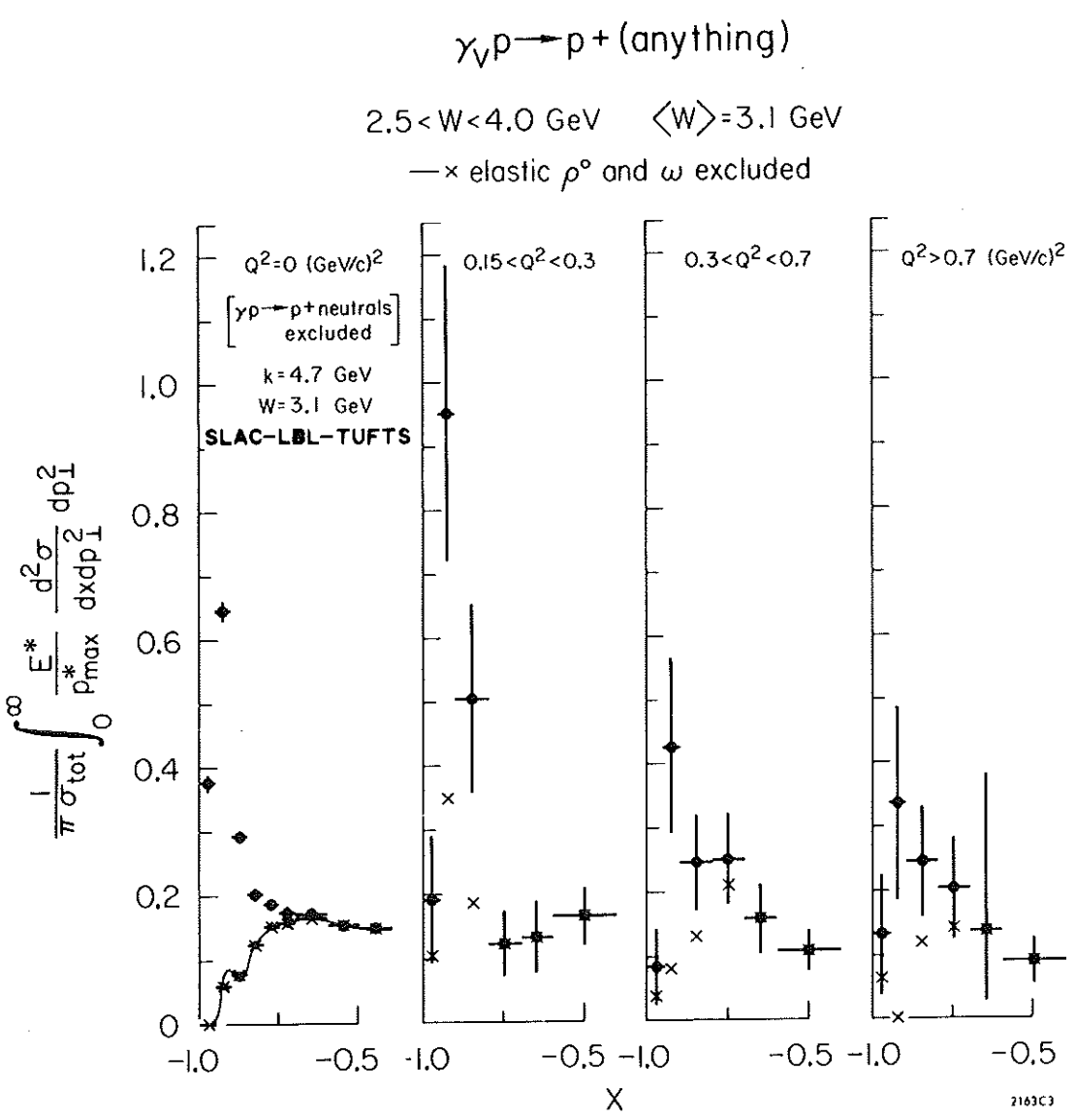
$\gamma_V p \rightarrow p + (\text{anything})$
$2.5 < W < 4.0$ GeV $\quad \langle W \rangle = 3.1$ GeV
— × elastic ρ^0 and ω excluded
$Q^2 = 0$ (GeV/c)^2
[$\gamma p \rightarrow p +$ neutrals excluded]
k = 4.7 GeV
W = 3.1 GeV
SLAC-LBL-TUFTS
$0.15 < Q^2 < 0.3$
$0.3 < Q^2 < 0.7$
$Q^2 > 0.7$ (GeV/c)^2
$\frac{1}{\pi \sigma_{tot}} \int_0^\infty \frac{E^*}{p^*_{max}} \frac{d^2\sigma}{dx dp_T^2} dp_T^2$
X
2163C3

Fig. 35

DESY

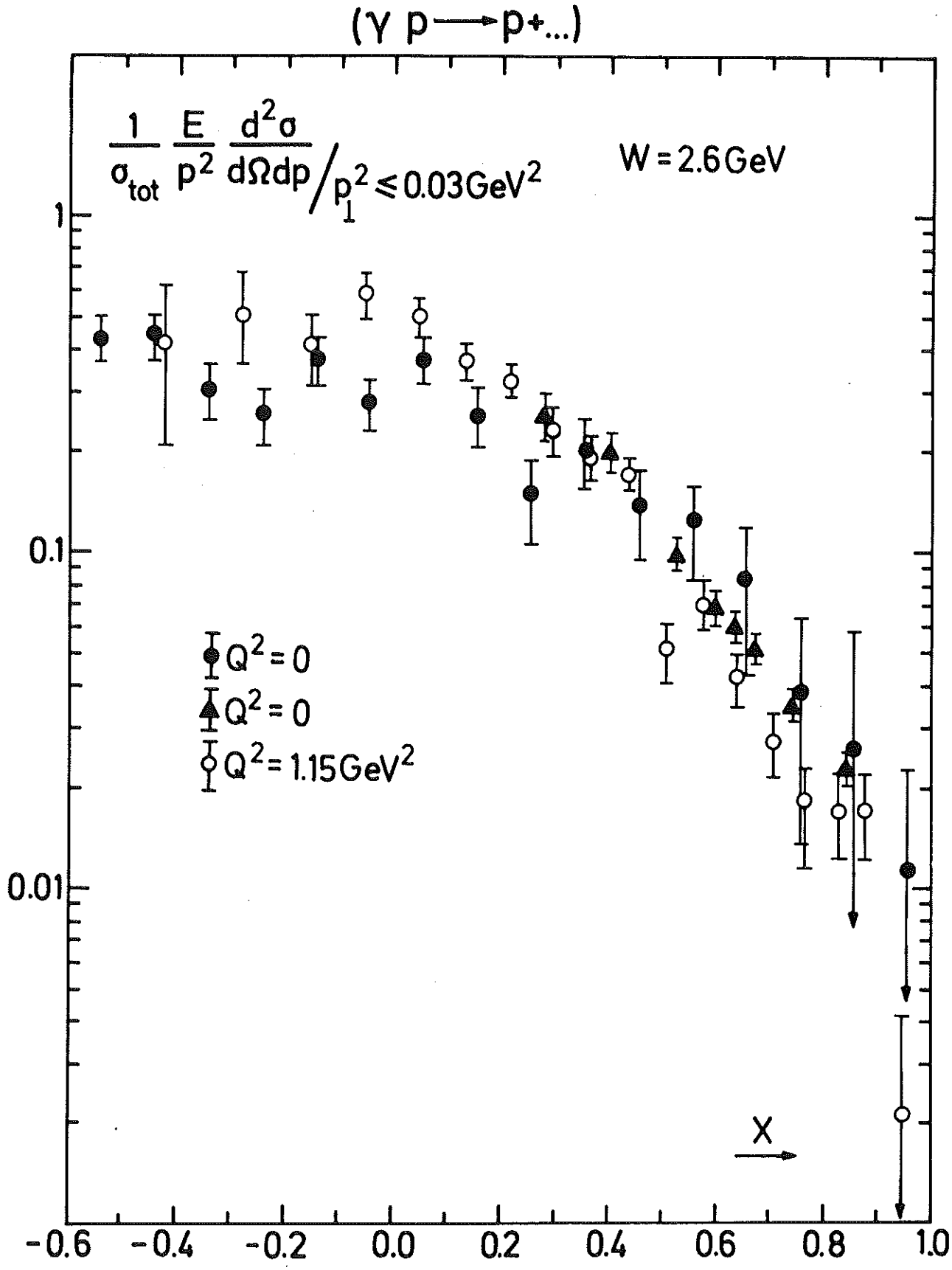
(γ p ⟶ p+...)
1/σ_tot E/p² d²σ/dΩdp / p_l² ≤ 0.03GeV²
W = 2.6GeV
1
0.1
0.01
Q² = 0
Q² = 0
Q² = 1.15GeV²
X
-0.6
-0.4
-0.2
0.0
0.2
0.4
0.6
0.8
1.0

Fig. 36